Quaternary Science Reviews 196 (2018) 137–153

Contents lists available at ScienceDirect

Quaternary Science Reviews

journal homepage: www.elsevier.com/locate/quascirev

The effects of mid-Holocene fluvio-eolian interplay and coastal dynamics on the formation of dune-dammed lakes in NE Brazil

André Zular [a, *], Giselle Utida [a], Francisco W. Cruz [a], André O. Sawakuchi [a], Hong Wang [b, c, d], Márcia Bícego [e], Paulo C.F. Giannini [a], Selma I. Rodrigues [f], Guilherme P.B. Garcia [a], Mathias Vuille [g], Abdel Sifeddine [h, i], Renata Zocatelli [j], Bruno Turcq [i], Vinícius R. Mendes [a]

[a] Instituto de Geociências, Universidade de São Paulo, Rua do Lago 562, São Paulo, 05508-080, Brazil
[b] State Key Laboratory of Loess and Quaternary Geology, Institute of Earth Environment, Chinese Academy of Sciences, Xian, Shaanxi, 710061, PR China
[c] Interdisciplinary Research Center of Earth Science Frontier, Beijing Normal University, Beijing, 100875, PR China
[d] Illinois State Geological Survey, Prairie Research Institute, University of Illinois at Urbana-Champaign, Champaign, IL, 61820, USA
[e] Laboratório de Química Orgânica Marinha, Instituto Oceanográfico, Departamento de Oceanografia Física, Universidade de São Paulo, São Paulo, Brazil
[f] Pró-Reitoria, Universidade de São Paulo, São Paulo, Brazil
[g] Department of Atmospheric and Environmental Sciences, University at Albany, SUNY, 1400 Washington Ave., Albany, NY, 12222, USA
[h] LMI PALEOTRACES (IRD UFF SORBONNE UNIVERSITÉ UPCH UANTOF), Departamento de Geoquimica, Niteroi, Brazil
[i] IRD-Sorbone Universités (UMR LOCEAN, Centre IRD France Nord), Bondy, France
[j] Université d'Orléans, Institut des Sciences de la Terre d'Orléans (ISTO), UMR 7327, CNRS/INSU, 45075, Orléans, France

ARTICLE INFO

Article history:
Received 5 August 2017
Received in revised form
11 July 2018
Accepted 15 July 2018
Available online xxx

Keywords:
Dune-dammed lakes
Paleoclimate
Coastal eolian deposits
Fluvio-eolian interplay
Boqueirão lake

ABSTRACT

We analyzed the Late Quaternary coastal evolution of the easternmost tip of South America in Brazil in light of fluvial-eolian interactions controlled by relative sea-level, climate, and coastal physiography changes. The chronology obtained by OSL-SAR of 36 samples coupled with sedimentological analysis from stabilized dunes suggest that eolian activity was primarily controlled by episodes of sediment availability because prevailing SE trade winds have been steadily strong throughout the Holocene. Contrary to the most conventional view linking dune activity to aridity, dune buildup occurred in a period of increased humidity in NE Brazil between 11 ka and 6 ka when a rising relative sea level and higher rainfall enhanced sediment delivery benefiting the construction of transgressive dunefields. The interplay of these advancing dunes with the existing drainage pathways is here investigated using a modern regional analog and through the evolution of Boqueirão Lake formed by dune blockage. Analysis of a sediment core from this lake dated between 8.4 and 0.9 ka indicated changes over time in microfossil assemblages, organic geochemistry, and grain size data conforming to fluvial or lacustrine depositional conditions. Between 7.2 and 4.4 ka, during the predominantly regional humid climate, the high abundance of fluvial sponge species correlated with a framework of competent-flow drainage systems diverting from advancing dunes. An abrupt transition from a wetter to a drier climate at 4.4–4.0 ka stimulated episodes of fluvial damming as indicated by sharp changes from sandy to muddy sediments and anomalous concentration of sponge spicules concurrent with significant mortality rates of fluvial adapted species. From 3.9 ka to the present, the disappearance of sponge spicules and peaking diatom concentration attested to a predominant lacustrine environment. Thus, the formation of Boqueirão Lake is mainly a result of the regionally drier climate and not a consequence of increased humidity in coastal NE Brazil.

1. Introduction

Advancement or diversion of sand dunes on lakes and rivers has been previously reported in many Late Quaternary studies (e.g., Langford, 1989; Langford and Chan, 1989; Bullard and

* Corresponding author. Luminescence and Gamma Spectrometry Laboratory, Instituto de Geociências, Universidade de São Paulo, Rua do Lago 562, 05508-080, São Paulo, SP, Brazil.
E-mail addresses: andrezular@gmail.com, andrezular@usp.br (A. Zular).

https://doi.org/10.1016/j.quascirev.2018.07.022
0277-3791/

McTainsh, 2003; Kadlec et al., 2015; Liu and Coulthard, 2015, 2017; Roskin et al., 2017). When facing advancing dunes, rivers and lakes are subject to competing eolian, fluvial, and lacustrine processes that result in diverse types of interactions (Al-Masrahy and Mountney, 2015 and references therein). Notably, a common type of fluvio-eolian interaction is associated with dune advancements over drainages resulting in the formation of natural dams. Most studies on the formation and evolution of this type of lake have been conducted on continental environments such as the Nebraska Sand Hills in the United States (e.g., Loope et al., 1995, 2004; Mason et al., 1997; Loope and Swinehart, 2000; Schmieder et al., 2012), and in dryland environments (e.g., Teller and Lancaster, 1986; Bullard and Livingstone, 2002; Hollands et al., 2006). In contrast, the interplay of fluvio-eolian processes on marine coastal environments has remained poorly documented, albeit lakes formed by dune-blockage in the littoral and nearby zones have been acknowledged in biological, geomorphological, and paleoclimatic studies (e.g., Arthington et al., 1986; Illenberger, 1996; and Sifeddine et al., 2003; respectively). Some of the very few studies on fluvio-eolian interplay in coastal environments have been conducted in coastal Namibia (e.g., Krapf et al., 2003; Svendsen et al., 2003; Garzanti et al., 2014; Al-Masrahy and Mountney, 2015; Krapf, 2018). These authors report on fluvial systems that hinder eolian sand encroachments, and on fluvio-eolian interactions in the Skeleton Coast controlled by the size of river catchments where dunes block ephemeral river systems on their path to the Atlantic Ocean. However, there is a paucity of knowledge about the chronology and fluvio-eolian interactions on coastal dune-dammed lakes associated with two of the main forcings that regulate the evolution of coastal plains: relative sea level and climate.

Coastal dunes adjacent to fluvial systems and lakes are widespread on the coast of Rio Grande do Norte State, NE Brazil (RN; Fig. 1a and b). This coast is dominated by active and stabilized dunefields, intermittent and ephemeral small coastal rivers, marshes, and a large number of shallow lakes (water depth < 10 m). However, the chronology of the development of this landscape and its response to relative sea-level and climate changes are poorly constrained. Also, there has been an emphasis on investigating the regional lacustrine or eolian archives separately (e.g., Sifeddine et al., 2003; Tsoar et al., 2009; respectively). For example, studies from lacustrine records of Boqueirão Lake, situated on the western boundary of the study area (Fig. 1b) suggest that current and past water levels were a function of rainfall alone (Zocatelli et al., 2012; Gomes et al., 2014; Viana et al., 2014). However, because this lake lies in the lee of stabilized dunes formed by strong winds, hydrological alterations to the lake and associated river pathways were likely to occur during episodes of dune activity.

In this study, we investigated fluvio-eolian interactions on the RN coast in the late Quaternary resulting from sea-level and climate changes. Because this region experienced substantial fluctuations in precipitation throughout the Holocene (Cruz et al., 2009; Montade et al., 2014; Mulitza et al., 2017) concurrent with a relative sea-level rise and highstand (Milne et al., 2005), we had a unique opportunity to assess the response from eolian and lacustrine systems to these changes. By investigating the Boqueirão Lake Holocene evolution in light of past and current fluvio-eolian interactions and sediment supply, we questioned the hypothesis that precipitation alone controls the water level of this lake. To tackle this task, we studied the coastal sediment pathways and cycles using a modern analog, and associated data obtained from the chronology and sedimentology of stabilized sand dunes to microfossil and sedimentological analysis of a Boqueirão Lake sediment core and seismic reflection profile.

2. Study area

2.1. Geomorphic setting

The investigated coastal area is located at the easternmost tip of South America (Fig. 1a inset). This area encompasses 50-km of coastal stretch followed by 590 km^2 of extensive NW-trending active and stabilized dunefields along with fluvial and lacustrine systems (Fig. 1b). This coastal section presents a negative sediment budget in a wave-dominated system where sediments are transported northward by alongshore currents and onshore by waves. These conditions promote beach erosion and support the local development of coastal dunes (e.g., Vital et al., 2004; Bittencourt et al., 2005). Eroding cliffs or dissipative sandy beaches are frequently cut by small ephemeral river mouths that are diverted (Fig. 2a) or blocked by coastal dunes forming ephemeral and permanent shallow lakes fed by small drainages (Fig. 2b). Also, low-lying marshes are bounded by dune fronts (Fig. 2c). A conspicuous feature of the study area is the clear morphology of active and stabilized dunefields. Even when physically degraded, these dunes show an SE-NW elongation direction. NW-oriented dune advancement trails or streaks are not discernible farther than 20 km from the coast where they are in part bounded by the SW- to NE-oriented sigmoidally-shaped Boqueirão Lake that lies in the Boqueirão River pathway (Fig. 2c). Boqueirão Lake is situated 13.5 km from the eastern RN coast and presents a maximum length, width, depth, and volume of 7 km, 0.6 km, 10 m, and 11,075 m^3, respectively (Gomes et al., 2014). Also, this lake lacks contribution from the 30-m depth groundwater (Diniz Filho et al., 2005). Its western edge is bounded by laterites crusts, sands, and finer sediments from the Barreiras and Post-Barreiras Neogene Formations (e.g., Angelim et al., 2006), and presents various zones with concave-shaped encroachments pointing to the NW. These features are not detected on the eastern lake margin that is bounded solely by paleodunes.

Regionally, the shallow nearshore and continental shelf environments are delineated by beach rock ridges (Fig. 1a; e.g., Vital et al., 2010, 2016). The identification of offshore beach rock lines was first established by remote sensing coupled with petrographic analyses of an elevated inner shelf ridge off the RN northern coast (Cabral Neto et al., 2010). We used a similar remote sensing approach to identify offshore beach rock ridges on the western coast (Supplementary Fig. A.1).

2.2. Climatic setting

The average yearly speed of the prevailing SE winds recorded at 50-m height is 8.5–9.0 m s^{-1} on the foreshore and 8.0 m s^{-1} on Boqueirão Lake (Fig. 1b; Amarante et al., 2003). The climate is tropical and humid with a mean annual temperature of 27 °C. Precipitation annually averages about 1200 mm and is mainly distributed from January to July resulting from the southerly shift of the Intertropical Convergence Zone (ITCZ) that peaks from March to May (Kousky, 1979).

3. Methods

3.1. Eolian sand dune analyses

3.1.1. Sampling

To assess the timing of dune activity and stabilization, samples for optically stimulated luminescence (OSL) dating were collected using light-protected hammered tubes. Samples for dose rate estimation were collected in plastic bags in the amount of 250–300 g. Eleven sediment samples were obtained at the frontal

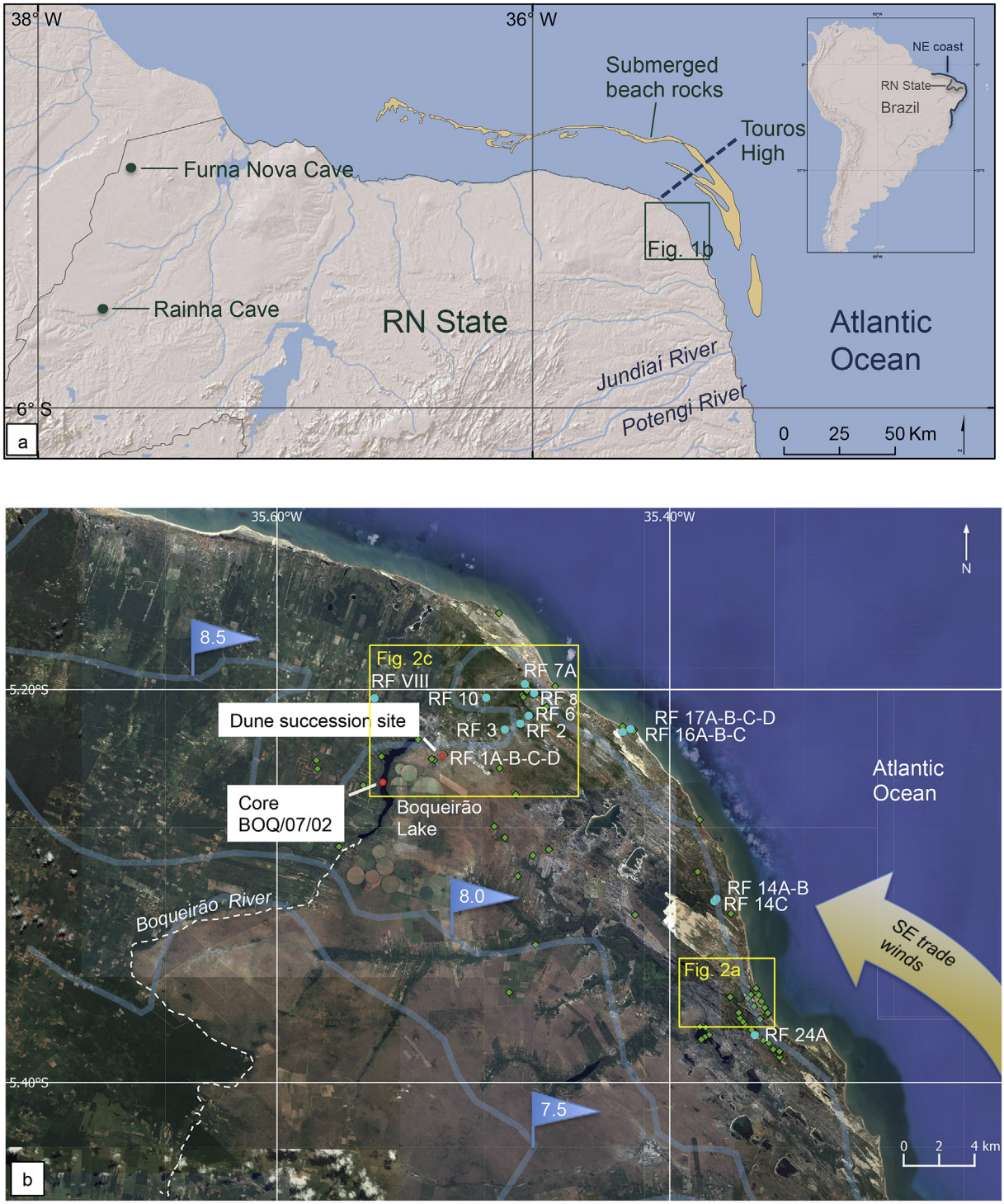

Fig. 1. The easternmost tip of the state of Rio Grande do Norte (RN). (a) Main locations mentioned in the text: regional rivers, caves, beach rock ridges, and the Touros High. The inset shows the location of RN and the northeastern region coastal stretch. Maps modified from GEBCO (2003). (b) The study area. Blue dots indicate OSL and sedimentological sample sites whereas blue lines and associated flags indicate current annual mean wind speeds in m s^{-1} at 50-m height (shapefile wind data: http://www.cresesb.cepel.br/index.php?section=publicacoes&task=livro&cid=1). The green diamonds mark control points that, together with the sampling locations are shown with site pictures on the Supplementary KMZ file. Also, the KMZ file shows the position of Fig. 2b. (For interpretation of the references to color in this figure legend, the reader is referred to the Web version of this article.)

lobe of stabilized parabolic dunes at depths of 1–3 m below the surface to avoid bioturbation and any remaining active dune crests (Fig. 1b and Supplementary KMZ file). To identify previous cycles of dune encroachment, we obtained eleven sediment samples at various depths in four profiles. Also, fourteen samples from a 7.8-m dune succession profile were obtained every 0.5–1.0 m. Preparation and cleaning-up for sampling this profile consisted of manually removing the talus slope and hollowing continuous adjacent vertical 0.7–1.0 m steps from top to bottom followed by outlining the fresh surfaces with 5-cm parallel divisions for the additional collection of samples for sedimentological analysis.

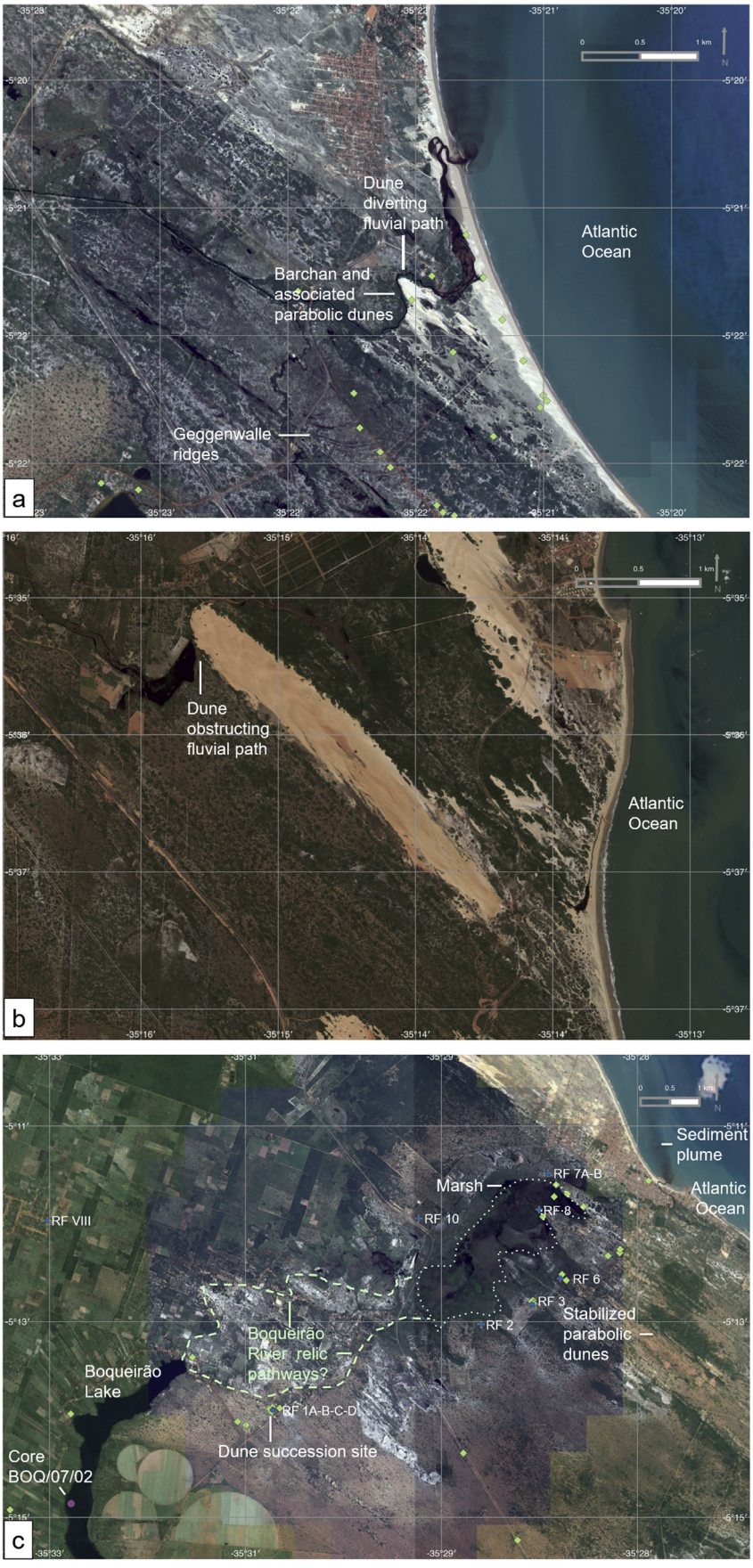
Dune diverting fluvial path
Atlantic Ocean
Barchan and associated parabolic dunes
Geggenwalle ridges
a
Dune obstructing fluvial path
Atlantic Ocean
b
Sediment plume
Marsh
RF 7A-B
RF 8
Atlantic Ocean
RF VIII
RF 10
RF 6
RF 3
RF 2
Stabilized parabolic dunes
Boqueirão River relic pathways?
Boqueirão Lake
RF 1A-B-C-D
Dune succession site
Core BOQ/07/02
c

3.1.2. OSL dating

The OSL dating method using the single-aliquot regenerative (SAR) dose protocol (Murray and Wintle, 2003) was applied to multigrain quartz aliquots to determine sediment burial ages. Samples were prepared in the laboratory under subdued red/amber light, according to procedures described by Aitken (1998). The 180–250 μm grain size fraction was obtained by wet sieving, followed by chemical treatment with 27% H_2O_2 and 10% HCl to remove organic compounds and carbonates, respectively. Quartz grains (2.65 g cm^{-3}) were isolated from heavy minerals and feldspar grains through gravity settling in lithium metatungstate solutions at a density of 2.75 g cm^{-3} and 2.62 g cm^{-3}, respectively. Subsequently, the quartz concentrates (2.75–2.62 g cm^{-3}) were treated with 48–51% HF for 40 min to remove remnant feldspar (especially plagioclase) and outer rinds of quartz grains dosed by alpha particles.

Aliquots of ~1000 grains were mounted with Sikospray silicone oil on monolayer aluminum discs using a 5 mm diameter mask for equivalent dose determination. Because of a large number of grains in the disk, we expected an underestimation of the values of overdispersion in the equivalent dose distribution (OEDD); large aliquots are prone to contain more dim or low sensitivity grains, though the remaining bright grains may produce results that pass the criteria for aliquot acceptance (Cunningham et al., 2011).

Luminescence measurements were carried out on Risø DA-20 TL/OSL readers with built-in beta source dose rate of 0.134 Gy s^{-1} and 0.088 Gy s^{-1} from the Illinois State Geological Survey (ISGS) and the Institute of Geosciences at the University of São Paulo (IGc-USP), respectively. Dose recovery tests were performed on bleached aliquots; bleaching was achieved by 3 h of sun exposure. These tests were done with a pre-heat temperature of 200 °C and given doses of 140, 52, and 4 Gy on samples RF 1A, RF 1B, and RF 1C, respectively. The equivalent dose for each sample was determined by measuring 24 quartz aliquots subjected to a four- or five-point SAR-OSL sequence (Supplementary Table B.1). The equivalent dose was calculated by exponential fitting of the dose-response data only when the recycling ratio was in the 0.9–1.1 range, and recuperation lower than 5%. Feldspar contamination was examined by repeating the first regeneration dose and using infrared stimulation at 60 °C before the blue stimulation. Aliquots were rejected when an infrared stimulated luminescence signal was detected, or when the OSL signal was depleted following infrared stimulation. The equivalent dose was determined through the central age model (Galbraith et al., 1999) using at least 16 accepted quartz aliquots per sample.

To calculate dose rates, mean specific activities (Bq kg^{-1}) of ^{238}U, ^{232}Th, and ^{40}K radionuclides were assessed using an HPGe detector (energy resolution of 2.1 KeV and relative efficiency of 55%) in an ultra-low background shield at the IGc-USP after keeping the samples sealed in plastic containers for at least 28 days for radon equilibration. Conversion factors of Guérin et al. (2011) were used for beta and gamma dose rates calculation. The cosmic dose rate was evaluated using sample depth below surface, altitude, longitude, and latitude (Prescott and Stephan, 1982). Moisture content was obtained from the water weight relative to dry sample weight after drying the samples in an oven for 48 h at 110 °C. The final ages were produced by dividing the equivalent dose value by the dose rate value.

3.1.3. Grain size and heavy mineral analyses

Bulk samples were examined on the optical microscope and subjected to grain-size analysis using a Malvern Mastersizer 2000 laser diffraction granulometer with a Hydro 2000MU attachment and a built-in ultrasound device. Grain size data were presented through descriptive statistics such as mean diameter and standard deviation and tabulated in 1-phi interval classes and classified according to Wentworth (1922). Samples for OSL-dating from the dune succession profile, foreshore, and foredunes, were analyzed for heavy minerals. For this analysis, the very fine sand fraction (62–125 μm) was separated by gravity-settling in bromoform ($CHBr_3$, density 2.83–2.89 g cm^{-3}) and placed on glass slides using Canada balsam for optical study under the polarizing microscope. Three hundred non-micaceous transparent heavy mineral grains plus opaque grains were counted through the ribbon method (Galehouse, 1971). Minerals were represented as a percentage of grains within the heavy minerals assemblage.

3.2. The Boqueirão Lake sediment core analysis

The 2.85-m long BOQ/07/02 sediment core was collected from Boqueirão Lake (5°14′52.5″ S, 35°32′48.2″ W, 17 m asl) at the IP21 seismic profile path using a vibracore pipe (Zocatelli et al., 2012, Fig. 3a and b). In the laboratory, the core was cut into 1 cm and 5 cm increments, between 5-160 cm and 161–285 cm depth ranges, respectively, for the following analysis: (a) microfossil identification and quantification of taxa assemblages; (b) organic geochemistry; (c) radiocarbon dating; (d) grain size distribution analysis; and (e) assessment of sediment color based on the Munsell Soil Color Chart (1992). All samples were stored at ~5 °C to avoid decomposition and degradation of microfossils. Subsequently, organic matter and carbonate were extracted from 1 cm^3; of each sample using 30–35% H_2O_2, and 37% HCl, respectively (Battarbee, 1986). Residual samples were cleaned and diluted in 50 ml of distilled water. Coverslips of 24 × 32 mm received 20 μl of this residue that was dried and glued to slides with Entellan®. Results were expressed in microfossils cm^{-3} of sediment (Stevenson and Rollins, 2006). Ten grams of each bulk sample were treated overnight with 10% HCl to eliminate carbonates for total inorganic carbon appraisal. Total organic carbon (TOC), total nitrogen (TN), carbon and nitrogen isotopes were then assessed using a Finnigan Delta V Plus Mass spectrometer coupled with a Costech Elemental Analyzer. TOC, carbon, and nitrogen isotopes were calibrated against laboratory standards, and against total inorganic carbon for TOC and carbon isotopes. Calibrated TOC and TN percentages were used to calculate the C/N ratio. Carbon and nitrogen isotopes were calculated in percentages per mil deviation, from the Vienna Pee Dee Belemnites (VPDB) and AIR standards, and represented by $\delta^{13}C$ and $\delta^{15}N$, respectively. Samples for radiocarbon dating were analyzed using the accelerator mass spectrometry (AMS) technique at the Laboratoire de Mesure du Carbone 14 (SacA, four samples) and the AMS Arizona Laboratory (AA, four samples). Radiocarbon ages were calibrated with CALIB 7.1 software using the SHcal13 model curve (Hogg et al., 2013), and reported as cal BP (2σ). An age model was determined by linear regression analysis using the average of the minimum and the maximum calibrated age from each sample. Ages derived from the age model were denoted as ka (thousand years ago) for a straightforward comparison with optical

Fig. 2. Geomorphological features of the study area. (a) An active dune diverting a river pathway, and (b) blocking a fluvial pathway forming a small shallow lake. (c) Boqueirão Lake and possible past Boqueirão River pathways shown in dashed lines. The dotted line shows the position of a paleolake formed by dune blockage, though currently, this location is a marsh. Blue dots and green diamonds indicate sample sites and control points, respectively. (For interpretation of the references to color in this figure legend, the reader is referred to the Web version of this article.)

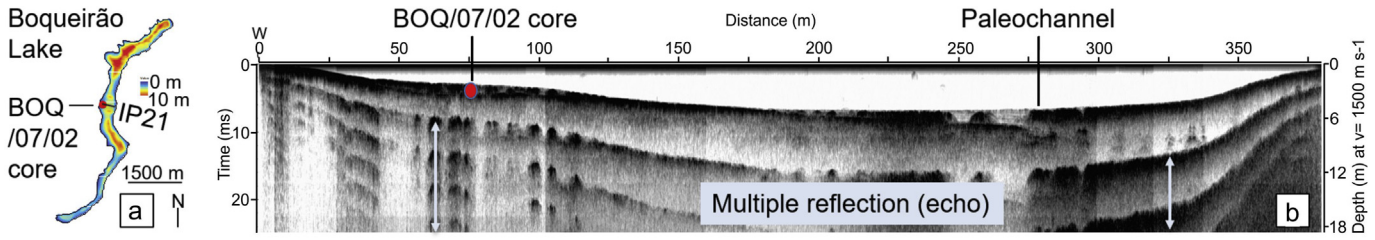

Fig. 3. (a) Boqueirão Lake bathymetric map showing the location of sediment core BOQ/07/02 on seismic profile IP 21. (b) The 10 kHz high-resolution IP21 seismic profile obtained at a sound velocity of 1500 m s^{-1} with depth-correction showing evidence of a paleochannel.

ages. Bulk samples for particle size distribution analysis followed the same method described in 2.1.3.

4. Results

4.1. The eolian dunefield record

All sampling locations presented unconsolidated sediments with at least 98% of quartz and absence of feldspar grains. Sand grains were mostly subrounded and showed surface textures with coatings. Zircon dominated the heavy mineral suite of the dune succession sands whereas rutile, tourmaline, kyanite, sillimanite, and staurolite were detected in minor frequency followed by traces of other minerals (Table 1a). In turn, sands from the foreshore and foredunes differed by their higher concentration of unstable heavy minerals represented by grains of pyroxene and amphibole (Table 1b).

The dose recovery test showed an average measured-to-given dose ratio between 0.94 ± 0.01 and 0.97 ± 0.01, indicating that our dating protocol worked well for the quartz aliquots extracted from the studied sediments. Luminescence measurements revealed bright quartz grains with an OSL signal dominated by the fast component (Fig. 4a), and dose-response curves that followed a linear (low doses) or exponential growth (Fig. 4b). Aliquots showed a recycling ratio between 0.93 and 1.08, indicating that changes in luminescence sensitivity were corrected properly. The median OEDD value was 24% (average = 22%; range of 5–42%; Table 2, Fig. 4c, d and f). This calculation excluded the uppermost massive layer of the dune succession (sample RF 180) that showed a 71% value. Even when considering an underestimation of the OEDD by values as high as 10%, our sediments would still mostly fall into the category of well-bleached sands (<35% OEDD; Arnold and Roberts, 2009). The equivalent dose results varied between 0.025 ± 0.004 Gy and 99.964 ± 4.222 Gy (Table 2).

Dose rate values derived from K, Th, and U (Table 2) showed a median value of 0.614 Gy ka^{-1} (average = 0.699 Gy ka^{-1}; range of

Table 1
Percentage of counted mineral grains in the heavy mineral suite. (a) Samples from the stabilized dune succession profile. (b) Samples from the present beach and foredunes.

	Site	Deposit	Sample #	zircon	rutile	staurolite	tourmaline	kyanite	sillimanite	andalusite	epidote	anatase	augite	hyperstene	granade	hornblende	amphibole
a	Dune succession profile samples	Eolian	RF 180	80	7	0	5	2	2	2	0	0	-	-	-	-	-
			RF 170	82	10	0	1	3	2	0	2	-	-	-	-	-	-
			RF 160	78	7	1	8	3	3	-	1	-	-	-	-	-	-
			RF 150	80	6	2	6	3	4	-	-	-	-	-	-	-	-
			RF 140	68	5	4	10	6	4	2	-	1	-	-	-	-	-
			RF 130	74	5	0	6	6	6	3	-	-	-	-	-	-	-
			RF 120	86	4	1	3	4	2	-	1	-	-	-	-	-	-
		Eolian coupled with alluvial/colluvial	RF 100	87	3	2	1	2	5	0	-	-	-	-	-	-	-
			RFB 25	85	5	-	3	4	2		1	-	-	-	-	-	-
			RFB 20	85	8	-	1	3	3	0	-	-	-	-	-	-	-
			RFB 1	90	4	-	1	2	2		0	-	-	-	-	-	-
			RFC 40	88	4	-	1	2	4	-	1	-	-	-	-	-	-
			RFC 20	89	4	-	1	3	2	0	1	-	-	-	-	-	-
			RFC 1	87	6	-	0	3	2	-	2	0	-	-	-	-	-
b	Beach and foredune samples	Beach	RF 32P	33	2	3	1	15	13	-	1	-	4	2	-	13	13
		Beach	RF 33P	12	1	10	1	18	15	-	5	-	5	6	-	14	13
		Foredune	RF 33DF	20	5	-	11	17	2	3	-	-	12	5	-	11	14
		Beach	RF 34P	5	-	5	-	23	4	-	3	-	16	10	1	17	15
		Foredune	RF 35DF	50	6	-	3	7	2	-	-	-	5	2	-	11	15
		Beach	RF 36P	14	1	1	5	15	12	-	-	-	9	10	-	17	16
		Foredune	RF 36DF	42	3	5	12	13	7	-	-	-	2	2	-	9	7

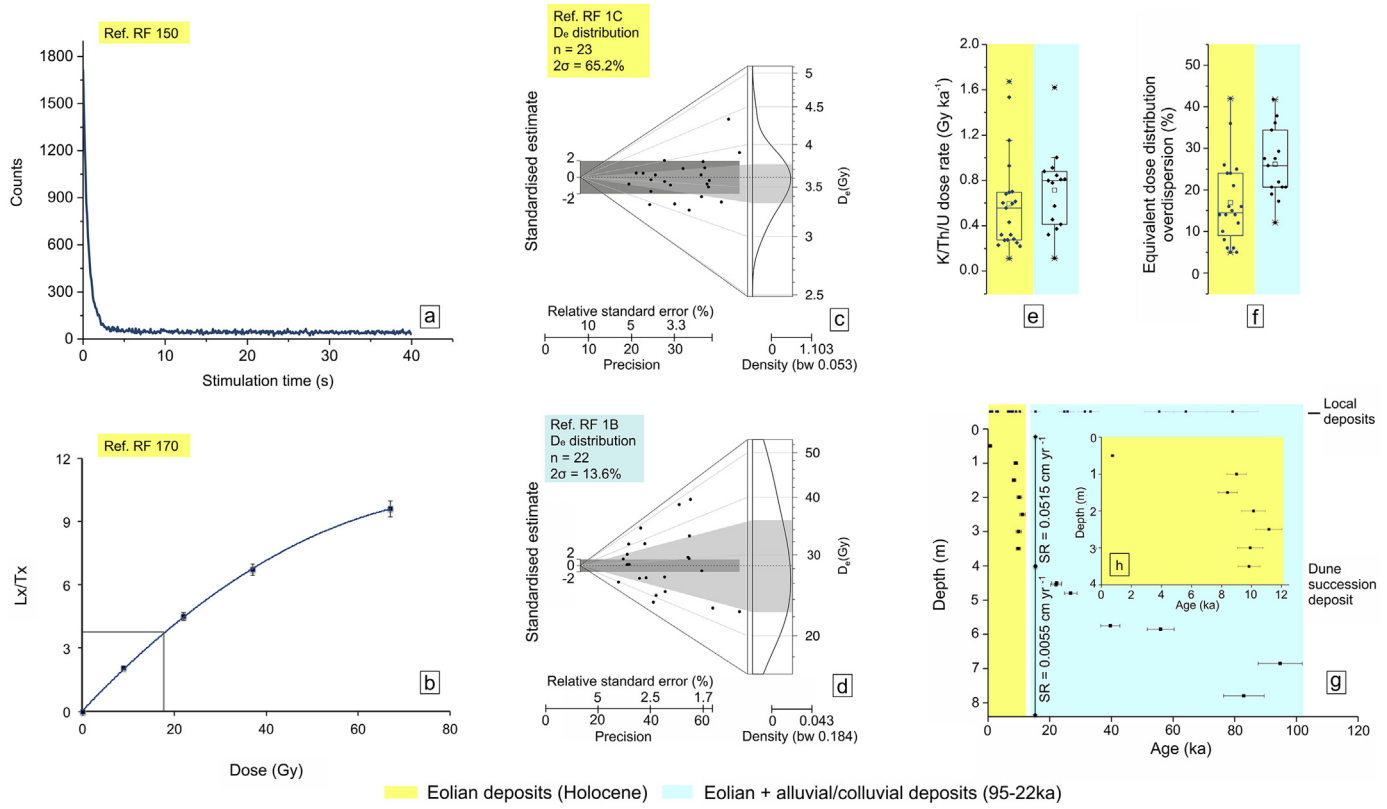

Fig. 4. Luminescence characteristics of quartz grains from the studied eolian deposits. (a and b) OSL decay curve from natural luminescence signal, and dose-response curve, respectively. (c and d) Abanico plots (Dietze et al., 2016) for equivalent dose (D_e)distribution. (e) and (f) Box plot graphs of K/Th/U dose rate and overdispersion of equivalent dose distribution, respectively. (g) Depth of accumulated sediment from the dune succession deposit over the last ~100 ka. To calculate the average sediment accumulation rate (SR) of overlapping ages (Holocene samples), the oldest and youngest age were associated with the bottommost and topmost sample depth, respectively. OSL ages from local deposits are shown on the top of the figure. (h) Magnified age-depth profile of the Holocene.

0.111–1.656 Gy ka^{-1}) whereas the K content median value was 0.021% (average = 0.081%; range of 0.004–0.612%). The low concentration of K, Th, and U led to a situation of a significant contribution (over 30%) of the cosmic dose rate to the total dose rate in many samples. For example, values as high as 37%, 48%, and 65% were estimated for samples RF 16B, RF 14C, and RF 6, respectively. OSL ages varied between 94.75 ± 7.16 ka and 0.06 ± 0.01 ka (Table 2; Fig. 4g; Supplementary Fig. A.2).

Although the OSL behavior of the studied quartz grains supports the calculation of reliable equivalent doses, the high contribution of the cosmic dose rate to the total dose rate requires additional evidence from our data to corroborate the soundness of our ages. A possible concern would be the occurrence of microdosimetric heterogeneities in the dose rate. We argue that all our sediment samples showed low potassium content (Table 2) that is consistent with the lack of feldspar in our mineral assemblage. Therefore, the bulk of the dose rate comes from U and Th radionuclides that originated from the prevalent zircon and rutile grains in the heavy mineral assemblage (Table 1a). These minerals incorporate U and Th radionuclides in their crystalline structure (Holland and Gottfried, 1955, and references therein). If these minerals were irregularly distributed in the sediments they could generate beta-dose heterogeneities affecting the dose rate. However, we believe that this was not a significant concern because of the relatively low OEDD, particularly for sands deposited between 11.2 ± 0.9 ka and 0.7 ± 0.1 ka (Fig. 4f). Also, sediments from this age range showed high textural and compositional maturity, as evidenced by the prevalence of moderately sorted unimodal fine quartz sands (Fig. 5a, b, and c). Thus, the use of 250–300 g of bulk sediment sample for gamma spectrometry measurements well represented radionuclide distribution surrounding the samples. Furthermore, our sediments lacked carbonates. Carbonates usually attenuate the effect of beta and gamma rays in the millimeter scale (e.g., Nathan and Mauz, 2008). These factors indicated that our homogeneous sediments would not be significantly affected by dose rate heterogeneity variations over time.

4.2. The Boqueirão Lake record

The uppermost 5 cm of the BOQ/07/02 core were not preserved probably because of the sampling method which induced compaction extending to the subsequent 20 cm. However, the remaining 265 cm of the core were not disturbed as we found no evidence of reworking, concavity, or bioturbation (Fig. 6a and Supplementary Fig. A.3). Between 5 and 45 cm, black silt grains lacking sedimentary structures were predominant (>60%; Fig. 6I). The interval between 45 and 125 cm was composed of 1-cm interbedded black and black-olive-gray silt layers (Fig 6II) where we detected *Biomphalaria* sp. shells. Between 125 and 139 cm, we found mainly black sediments that transitioned between silt and sand. In turn, gray-black-dark gray sands (>65%; Fig 6III) prevailed in the subsequent interval between 140 and 160 cm. Between 161 and 230 cm, we found a predominance of gray sands (>75%; Fig 6IV). The basal portion of the core, between 230 and 284 cm, was characterized by gray sediments composed of 40% sand, 50% silt, and 10% clay (Fig 6V).

Archived seismic reflection data of Boqueirão Lake show a flat bottom in its central area and continuous undeformed strata

Table 2
OSL dating data. Moisture content for all samples was between 3 ± 2% and 7 ± 4%, except for sample RF 6 that showed 17 ± 10%.

Method	Site	Deposit	Sample #	Depth (m)	Dose (Gy)	Approved aliquots	OD (%)	K (%)	Th (ppm)	U (ppm)	Gamma (Gy ka^{-1})	Beta (Gy ka^{-1})	Cosmic dose rate (Gy ka^{-1})	Total dose rate (Gy ka^{-1})	Age (ka)
OSL-SAR	Dune succession profile	Eolian	RF 180	0.50	0.804 ± 0.134	19	71%	0.014	6.390	2.020	0.522	0.407	0.161 ± 0.008	1.090 ± 0.043	0.74 ± 0.12
			RF 170	1.00	16.482 ± 1.072	18	15%	0.016	12.209	3.538	0.951	0.721	0.156 ± 0.007	1.828 ± 0.074	9.00 ± 0.65
			RF 160	1.50	14.204 ± 0.938	24	16%	0.015	10.602	3.392	0.864	0.669	0.151 ± 0.007	1.685 ± 0.069	8.40 ± 0.64
			RF 150	2.00	5.896 ± 0.402	24	14%	0.010	3.168	0.874	0.244	0.187	0.147 ± 0.007	0.578 ± 0.021	10.13 ± 0.78
			RF 140	2.50	5.226 ± 0.402	24	14%	0.007	2.351	0.654	0.182	0.139	0.143 ± 0.007	0.464 ± 0.017	11.15 ± 0.86
			RF 130	3.00	4.154 ± 0.268	24	12%	0.011	1.990	0.552	0.155	0.121	0.139 ± 0.006	0.415 ± 0.015	9.91 ± 0.84
			RF 120	3.50	4.154 ± 0.268	24	10%	0.013	1.989	0.577	0.158	0.126	0.135 ± 0.006	0.418 ± 0.015	9.83 ± 0.72
		Eolian coupled with alluvial/colluvial	RF 100	4.50	24.120 ± 1.608	24	34%	0.012	9.249	1.387	0.572	0.379	0.127 ± 0.006	1.078 ± 0.043	22.25 ± 1.66
			RFB 25	4.55	22.512 ± 1.474	24	29%	0.013	7.927	1.442	0.527	0.365	0.127 ± 0.006	1.018 ± 0.041	22.07 ± 1.71
			RFB 20	4.80	28.006 ± 1.876	23	20%	0.017	8.678	1.374	0.548	0.370	0.118 ± 0.005	1.036 ± 0.041	26.81 ± 2.06
			RFB 1	5.75	48.106 ± 3.216	23	24%	0.019	11.335	1.484	0.664	0.431	0.117 ± 0.005	1.212 ± 0.048	39.66 ± 3.09
			RFC 40	5.85	22.512 ± 1.474	24	35%	0.021	2.030	0.557	0.157	0.128	0.113 ± 0.005	0.399 ± 0.015	55.99 ± 4.35
			RFC 20	6.85	60.166 ± 4.020	24	25%	0.004	4.860	0.880	0.310	0.211	0.110 ± 0.005	0.632 ± 0.027	94.75 ± 7.16
			RFC 1	7.80	84.554 ± 2.546	24	33%	0.019	9.490	1.240	0.550	0.358	0.107 ± 0.005	1.016 ± 0.040	82.96 ± 6.60
	Local deposits	Eolian	RF 16B	0.50	0.025 ± 0.004	16	5%	0.114	1.121	0.315	0.117	0.153	0.163 ± 0.008	0.436 ± 0.026	0.06 ± 0.01
			RF 16C	0.25	0.088 ± 0.001	16	6%	0.205	3.998	0.828	0.333	0.353	0.164 ± 0.008	0.859 ± 0.061	0.10 ± 0.01
			RF 17D	0.30	0.080 ± 0.023	21	6%	0.159	0.629	0.176	0.088	0.158	0.163 ± 0.008	0.414 ± 0.026	0.19 ± 0.06
			RF 6	0.43	0.134 ± 0.001	16	36%	0.035	0.651	0.209	0.053	0.056	0.203 ± 0.010	0.314 ± 0.015	0.43 ± 0.02
			RF 7A	1.15	0.440 ± 0.001	16	16%	0.049	4.679	1.248	0.375	0.303	0.159 ± 0.008	0.841 ± 0.061	0.52 ± 0.03
			RF 8	0.77	0.736 ± 0.033	19	24%	0.064	3.660	0.969	0.298	0.255	0.162 ± 0.008	0.719 ± 0.050	1.02 ± 0.09
			RF 24A	1.00	1.144 ± 0.088	16	24%	0.140	1.483	0.302	0.138	0.178	0.160 ± 0.008	0.481 ± 0.030	2.38 ± 0.24
			RF 14C	0.70	1.206 ± 0.001	21	21%	0.087	0.855	0.289	0.094	0.123	0.202 ± 0.010	0.422 ± 0.023	2.86 ± 0.15
			RF 2	0.57	4.752 ± 0.176	24	26%	0.024	4.431	1.102	0.335	0.255	0.162 ± 0.008	0.757 ± 0.053	6.28 ± 0.50
			RF 3	0.55	5.935 ± 0.310	24	25%	0.050	5.336	1.159	0.392	0.304	0.162 ± 0.008	0.863 ± 0.062	6.88 ± 0.61
			RF 1D	1.00	10.452 ± 0.402	23	14%	0.007	8.253	2.701	0.694	0.536	0.200 ± 0.010	1.353 ± 0.093	7.73 ± 0.61
			RF VIII	1.00	5.628 ± 0.268	20	8%	0.017	4.403	1.142	0.341	0.258	0.160 ± 0.008	0.762 ± 0.053	7.38 ± 0.62
			RF 1C	3.50	3.618 ± 0.134	23	5%	0.026	1.385	0.439	0.119	0.105	0.185 ± 0.009	0.414 ± 0.022	8.75 ± 0.57
			RF 14B	0.40	8.174 ± 0.402	17	42%	0.113	4.192	0.831	0.320	0.287	0.204 ± 0.010	0.818 ± 0.054	9.99 ± 0.82
		Eolian coupled with alluvial/colluvial	RF 17C	0.60	11.444 ± 0.722	17	26%	0.245	2.875	0.597	0.262	0.326	0.162 ± 0.008	0.759 ± 0.053	15.08 ± 1.43
			RF 1B	4.80	29.078 ± 1.072	22	28%	0.012	9.301	1.515	0.601	0.403	0.178 ± 0.008	1.190 ± 0.086	24.43 ± 1.98
			RF 16A	1.10	23.048 ± 0.804	23	23%	0.344	3.175	0.574	0.294	0.400	0.199 ± 0.010	0.904 ± 0.063	25.49 ± 1.99
			RF 10	2.36	23.316 ± 0.804	23	25%	0.004	4.830	0.879	0.329	0.225	0.191 ± 0.009	0.749 ± 0.051	31.12 ± 2.24
			RF 14A	3.70	36.314 ± 1.474	19	29%	0.153	7.048	1.138	0.494	0.416	0.184 ± 0.009	1.104 ± 0.079	32.89 ± 2.70
			RF 1A	6.40	99.964 ± 4.422	20	25%	0.021	16.687	2.378	0.992	0.646	0.154 ± 0.007	1.810 ± 0.134	55.22 ± 4.75
			RF 17A	4.20	72.052 ± 4.821	21	30%	0.612	3.115	0.622	0.361	0.605	0.145 ± 0.007	1.128 ± 0.089	63.86 ± 6.63
			RF 17B	3.50	49.312 ± 3.882	23	37%	0.234	1.786	0.461	0.193	0.276	0.149 ± 0.007	0.624 ± 0.043	78.98 ± 8.30

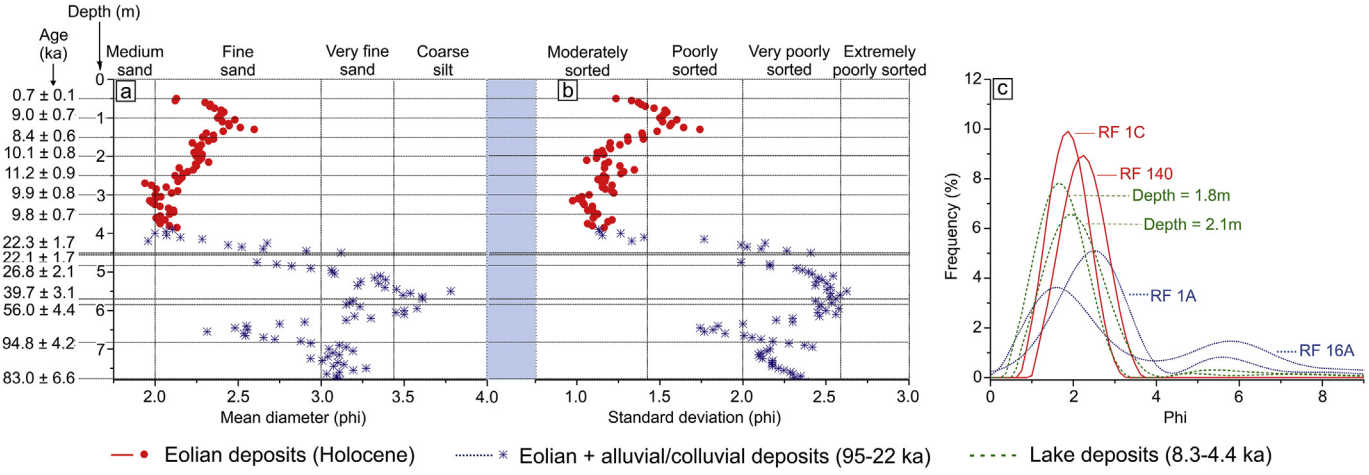

Fig. 5. (a and b) Mean diameter and sortness, respectively, of the dune succession samples distributed by depth and age. Classification of sands into sorting classes was based on standard deviation (Friedman et al., 1992). (c) Grain size-frequency distribution including lake deposit samples.

superimposed by a strong reflection thin layer (up to 1 m; Fig. 3b; Zocatelli et al., 2012). We observed a clear boundary between these layers throughout the lake. Also, diffuse and high amplitude reflections pointed to acoustic blanking characteristic of free gas. Sediments thickened towards the lake center, and shoulders showed erosional or depositional features. We detected terraced gently and more gently sloping surfaces in the western and eastern lake edges, respectively. Also, we observed an infilled paleochannel ~100 m from the eastern Boqueirão Lake edge.

The core BOQ/07/02 recorded sedimentation processes from ~8.4 to 0.9 ka (Table 3, Fig. 6a). Sponge spicules and diatoms were the most common siliceous microfossils. Spicules, mostly fragmented, were identified as megascleres (Demospongiae Class) because of straight or slightly curved oxeas, smooth or eventually expanded central areas, and gradual tapering extremities (Fig. 6c). Megascleres were registered from ~7.2 ka at a concentration of

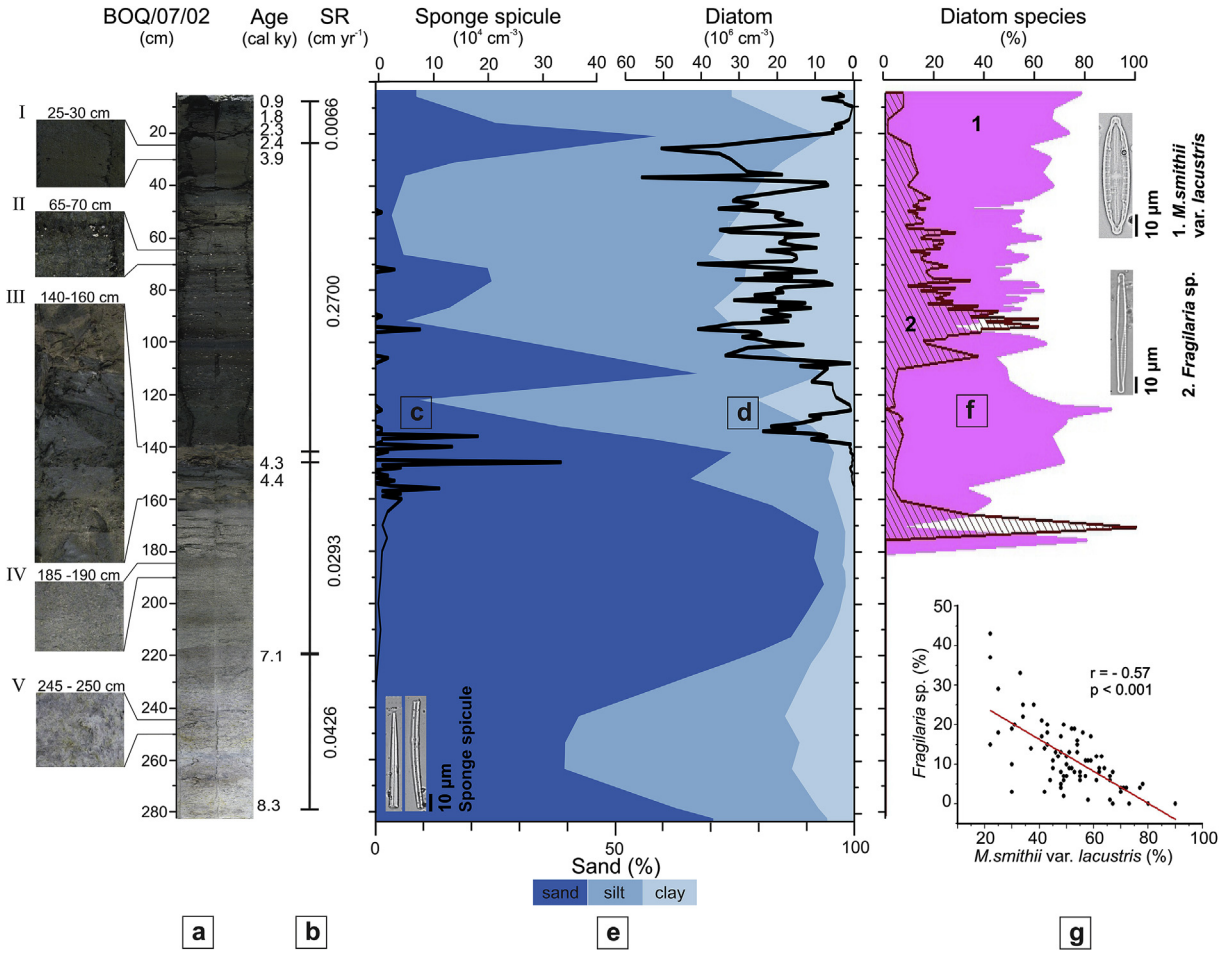

Fig. 6. (a) Stratigraphy of sediment core BOQ/07/02 from Boqueirão Lake with ^{14}C ages and associated data: (b) SR (sediment accumulation rate); (c) Sponge spicule density; (d) Diatom density; (e) Graphical representation of sand content in the core; and (f and g) Individual diatom species density and their correlation.

Table 3
Radiocarbon dating results.

Lab ID	Depth (cm)	$\delta^{13}C$	Age ^{14}C (BP)	Error	Minimum age (cal BP)	Maximum age (cal BP)	prob. 0,95 (2σ)	Average age (cal BP)
AA93417	10-.11	-25.7	1019	37	796	937	97.8	867
SacA35497	13-14	-26.64	960	30	760	918	100	839
SacA35498	15-16	-25.25	1845	30	1697	1825	87.3	1761
AA93424	20-21	-23.8	2325	36	2295	2356	57.1	2326
SacA35499	23-24	-23.3	2430	30	2340	2497	88.8	2419
AA93420	30-31	-26.9	3622	39	3811	3985	85.1	3898
AA93416	40-41	-27.6	3598	41	3708	3872	100	3790
AA93422	45-46	-27.3	4022	45	4285	4573	98.9	4429
AA93421	80-81	-25.4	3703	40	3862	4084	97.4	3973
AA93425	90-91	-26.9	4075	49	4407	4654	89.2	4531
AA93415	110-111	-23.8	3730	49	3871	4155	99.2	4013
AA93423	120-121	-23.1	3738	38	3905	4150	100	4028
AA93426	130-131	-23.7	3720	38	3890	4100	93.8	3995
AA93418	148-149	-22.1	3929	42	4217	4424	90.2	4321
SacA35500	154-155	-13.59	4025	30	4383	4530	94.2	4457
AA93419	230-231	-26.08	6262	63	6951	7267	100	7109
SacA35500	255-256	-19.79	5885	40	6527	6749	97.7	6638
SacA35502	280-281	-19.88	7520	70	8166	8414	100	8290

10^3 cm^{-3} and peaked at ~4.4 ka to 33.6 10^4 cm^{-3}, at times of predominantly sand deposition (Fig. 7g and h) under a sediment accumulation rate of 0.0293 cm yr^{-1} (Fig. 6b). The $\delta^{13}C$, $\delta^{15}N$, and C/N records were missing on the sandy bottom layers in the ~6.5–4.8 ka interval, thus indicating little organic fractions (Fig. 7c, d, and e, respectively).

About 40% of the lake sediment sequence was deposited in a short time between ~4.4 ka and 3.9 ka. The high sediment accumulation rate of 0.2700 cm yr^{-1} originated a series of superimposed radiocarbon dates as observed between the depth of 154–155 and 30–31 cm (Table 3). These overlapping ages were at least in part affected by sediment reworking as evidenced by the

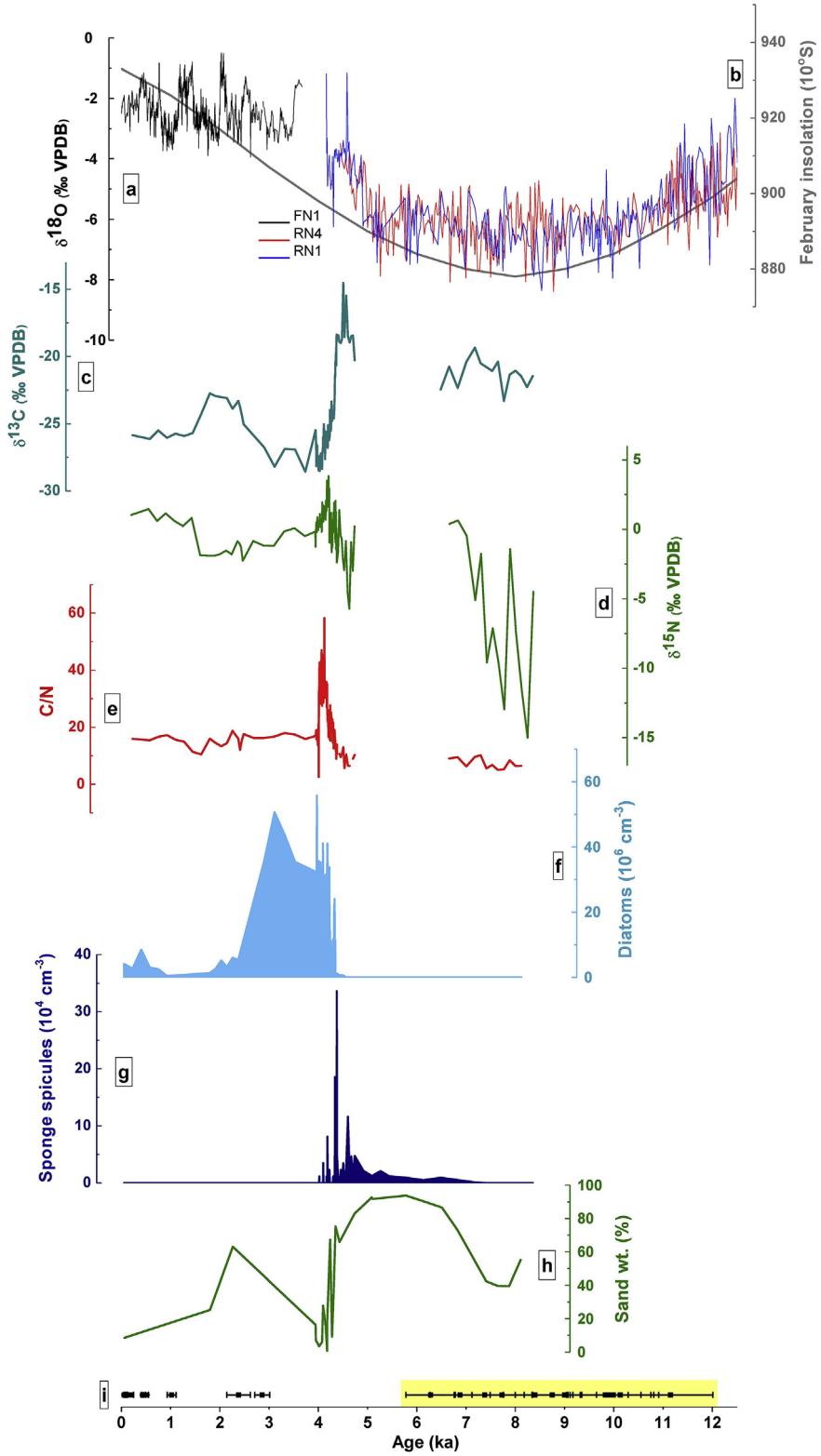

Fig. 7. (a) Oxygen isotope data of speleothems from Northeastern Brazil (Cruz et al., 2009). (b) February insolation at 10°S. Boqueirão lake core data: (c) Carbon isotope; (d) Nitrogen isotope; (e) C/N ratio; (f) Diatom density; (g) Sponge spicule density; (h) Sand content; and (i) Dune chronology data. The highlighted band corresponds to the transgressive dunefield formation from the mid-to late Holocene.

sand fraction decreasing in a zig-zag fashion between 75% and 7% (Fig. 7h). Indeed, changes from fluvial to lacustrine environments during this period were evidenced by (a) megascleres concentration gradually decreasing, although lacking at times; (b) decreasing $\delta^{13}C$ values; and (c) increasing $\delta^{15}N$ and C/N values (Fig. 7g, c, d, and e, respectively). During this period, diatoms of the

species *Mastogloia smithii* var. *lacustris* and *Fragilaria* sp. were first detected (Fig. 6f). These species are characteristically lacustrine (Denys et al., 1991; Gaiser et al., 2010) and contributed to ~70% of the total diatom abundance (Fig. 6d). Also, we found a negative linear correlation between the concentration of these two diatom species ($r = -0.57$; Fig. 6g). The highest total diatom density of 55.7 10^6 cm^{-3} was synchronous with the disappearance of sponge spicules at ~3.9 ka under the sediment accumulation rate of 0.0066 cm yr^{-1} (Fig. 6d and b, respectively). Between 3.9 ka and 3.1 ka, diatom abundance remained relatively high. Subsequently, it decreased abruptly reaching the lowest value of 0.5 10^6 cm^{-3} at ~1.0 ka (Fig. 7f). The $\delta^{13}C$, $\delta^{15}N$, and C/N record remained relatively stable during the ~3.9–0.2 ka period under lacustrine conditions (Fig. 7c, d, and e, respectively).

5. Discussion

5.1. Dune activity

The determined OSL ages provide a reliable chronology for the dunes, which demonstrate that the RN coast was subjected to multiple episodes of sand deposition at least since ~95 ka (Table 2 and Supplementary Fig. A.3). Sediments deposited between 94.8 ± 7.1 ka and 22.3 ± 1.7 ka showed a low average sediment accumulation rate of 0.0055 cm yr^{-1} (Fig. 4g). Also, they presented very poorly sorted grains of a medium-silt mode coupled with a higher-magnitude sand mode (Fig. 5b and c) and granules (quantitative data not shown). This characteristic points to a contribution of eolian, alluvial, colluvial, or a combination of any of these processes to the sediment overburden during this period, making paleoenvironmental interpretations based only on OSL ages not straightforward. A plausible framework would entail an alluvial or colluvial contribution from the Barreiras and Post-Barreiras sediments to these deposits. Also, these sediments showed different luminescence characteristics when compared to the younger sediments such as higher average dose rate and OEDD (Fig. 4f and e, respectively). The higher OEDD of the sediments deposited between 94.8 ± 7.1 ka and 22.3 ± 1.7 ka were in the range or slightly higher than the limit attributed to well-bleached sediments (Arnold and Roberts, 2009). We hypothesize that these higher values may be related to partial bleaching, post-depositional sediment mixing (e.g., Lomax et al., 2007), microdosimetry effects resulting from heterogeneities in radionuclides distribution, or a combination of all these factors. In contrast, sediments deposited between 11.2 ± 0.9 ka and 0.7 ± 0.1 ka under the higher average sediment accumulation rate of 0.0515 cm yr^{-1} (Fig. 4g and h) consisted of unimodal moderately sorted fine sands (Fig. 5a, b, and c) pointing to an imprint of eolian deposition during this period. These sediments showed: (a) lower average OEDD values (<17%; Fig. 4f), excluding the exceptional 71% detected at the 0.5 m depth in the sediment section (Table 2). This value may be attributed to bio- or pedoturbation affecting grain mixing, as shown in other studies (e.g., Bateman et al., 2007; Rawling et al., 2008; Arnold and Roberts, 2009; Mason et al., 2011); (b) a lower average dose rate compared to the older sediments (Fig. 4e). Differences in the dose rate may be applied to discriminate sediments derived from diverse sources (e.g., Macdonald et al., 1997; Mohanty et al., 2004).

Eolian dune construction usually reflects optimal conditions of sediment supply, transport, and preservation, which may be interspersed with periods of erosion or sand bypass (e.g., Kocurek, 1999; Singhvi and Porat, 2008). However, we interpret the OSL ages between 11.2 ± 0.9 ka and 6.3 ± 0.5 ka as indicators of intense or pulsed dune activity. This is justified by a combination of regional landforms such as NW-oriented barchans, *gegenwalle* ridges (counter ridges formed opposite to the dominant wind; Hesp et al., 2011), and parabolic dunes showing on the near-surface the last recorded OSL ages in this period, between 6.9 ± 0.6 ka and 6.3 ± 0.5 ka (Refs. RF 2 and RF 3, respectively; Table 2). These ages are most likely related to the last stabilization event after a significant phase of dune construction. In the study area, the above-mentioned dune morphologies combine new sand advancements moving over older surfaces stabilized by vegetation. This framework is common in tropical coastal areas in Brazil (e.g., Buynevich et al., 2010) which are usually associated with the formation of transgressive dunefields (Guedes et al., 2017). There is much debate about the formation of these deposits and initiation mechanisms may include, for example, relative sea-level variations, climate change, or a contribution from both (Hesp, 2013 and references therein). We discuss the controls over the development and stabilization of eolian dunes in the study area in the following subsections.

5.1.1. The contribution of relative sea-level changes to sediment supply in coastal RN

In Brazil, the early Holocene is characterized by a relative sea-level rise that lasted until the mid-Holocene, when it peaked regionally between 1 and 4 m higher than present sea level (Angulo et al., 2006). Rising relative sea level induces coastal erosion that may supply abundant foreshore sediments to initiate transgressive dunefield development under high eolian energy conditions (e.g., Cooper, 1958; Pye and Bowman, 1984). In Australia, for example, transgressive dunes were formed between 10 and 6 ka (Pye and Bowman, 1984; Lees et al., 1993; Sloss et al., 2007). Modeling of relative sea-level data from the Caribbean and northeastern Brazil, which includes a site 300 km south of the study area, indicates relative sea-level rise rates of 7–8 mm yr^{-1} in the early Holocene (Milne et al., 2005). Also, analysis of samples from the Potengi River estuary (Fig. 1a) shows a relative sea-level rise rate of 6.1 mm yr^{-1} between 8.3 and 7.0 ka (Boski et al., 2015). It seems reasonable to suggest that relative sea-level rise may have contributed to supply sediments for the formation of a transgressive dunefield in the study area. This contribution may have lasted until the mid-Holocene when relative sea level began to fall and subsequently stabilized. This hypothesis is consistent with the present coastal environment in northeastern Brazil, formed after the Last Glacial Maximum when dissipative beaches were constructed. Processes that lead to the formation of dissipative beaches are varied and may include a combination of factors such as wave energy (e.g., Carter, 1990; Padilla and Alsina, 2017), or the occurrence of storms (e.g., Christiansen et al., 1990; Angnuureng et al., 2017), rather than a process that involves sediment supply only. Notwithstanding, this type of beach configuration often stores large quantities of sand in the shoreface (Roy and Thom, 1981; Pye and Bowman, 1984) that can ultimately fuel dune activity as shown by the rise in the sediment accumulation rate during the early Holocene in the study area (Fig. 4g and h).

The Holocene relative sea-level highstand of +1.3 m in the northern RN state was radiocarbon dated at ~6.3 ka using beach rock (Caldas et al., 2006). Although the meaning of beach rock dating is controversial (Murray-Wallace and Woodroffe, 2014), this age fits well with the subsiding dune activity at 6.28 ± 0.50 ka, thus indicating dune stabilization at times of diminishing sand supply after the maximum Holocene relative sea level.

5.1.2. The role of holocene climate variations in coastal RN dune activity

Marked changes in rainfall on millennial time scales affected NE Brazil during the Holocene (e.g., Novello et al., 2012; Bertrand et al., 2017). The Icatú River Valley (please refer to the Supplementary

KMZ file for location) provided the first evidence of changing climate during this period. In this area, the dominant semi-humid pollen taxa such as *Mauritia vinifera* attested to a bioma of cerrado vegetation during the early to mid-Holocene (De Oliveira et al., 1999). In turn, during the late Holocene these authors found pollen from semi-arid plants taxa typical of caatinga vegetation. Also, high-resolution stable oxygen isotope speleothem records from Rainha and Furna Nova Caves (Cruz et al., 2009) located nearby this study site (Fig. 1a) showed periods of enhanced precipitation during the early to mid-Holocene. These authors found more negative values of $\delta^{18}O$ between 10.5 and 5 ka, coeval with low summer insolation in the Southern Hemisphere (Fig. 7a and b).

Proxy records obtained recently from sediments of a marine core situated in front of the Parnaíba River catchment (GeoB16202-2; Supplementary KMZ file) support the Icatú River Valley and the Rainha and Furna Nova Cave climatic archive. Higher values of plant wax lipids from the GeoB16202-2 core indicated a drying climate from east to west on the NE Brazil coast during the last 5 ky (Mulitza et al., 2017). These authors showed a tendency towards a semi-arid climate during late Holocene reinforced by a weaker riverine input of sediments as suggested by a significant decrease in the Fe/Ca ratio. Additional evidence of climate change in NE Brazil during the Holocene comes from Serra de Maranguape (Supplementary KMZ file). At this location, significant compositional changes in forest types took place between ~5 ka and ~1 ka, attesting to regionally drier conditions (Montade et al., 2014). These changes in climate from mid-to late Holocene may reflect primarily a decrease in the equatorial rainfall induced by changes in the location of the Intertropical Convergence Zone on the northern coast of NE Brazil (Cruz et al., 2009; Mulitza et al., 2017).

Regional wind conditions in the early Holocene are not well established on the RN coast, though currently strong winds occur all year round. The wet and dry seasons register average speeds that are sustained farther inland than Boqueirão Lake, of 6 m s^{-1} and 9 m s^{-1}, respectively (Amarante et al., 2003, Fig. 1b). It is plausible that such wind speeds were maintained during the early Holocene because sediments from the foreshore were transported in significant amounts over even longer distances from the early Holocene coastline to Boqueirão Lake.

Varying rain and wind conditions affect eolian sediment supply and mobility (e.g., Hugenholtz and Wolfe, 2005). For example, on the low gradient 40-km narrow RN state continental shelf enhanced storminess brings more wave erosion and sediment availability (Vital et al., 2004). Also, increased precipitation stimulates fluvial erosion of stabilized dunes or soils covering bedrocks in association with enhanced sediment transport by rivers. These sediments may ultimately end up in the foreshore as shown elsewhere (e.g., Suanez et al., 2013; Harley et al., 2017). In the Curumataú River estuary, RN state (Supplementary KMZ file), river discharge increases substantially during periods of heavy rains (De Miranda et al., 2005). There are no regional studies on how this affects the sediment load transported by rivers or by longshore drift currents in our study area. In comparison, a coastal area of seasonal rains showing similar average annual precipitation in southern Brazil (the Itajaí-Açu River; Supplementary KMZ file) produced an enhanced sediment load during continuous rains (Schettini and Toldo, 2004).

Considering that the primary period of dune buildup in the study area during the Holocene (~11.2–6.3 ka) is synchronous with the wetter regional climate (~10.5–5 ka), we rule out aridity-driven changes in vegetation cover as one of the primary controls on dune dynamics. Accordingly, in addition to the sediment contribution provided by the relative sea-level rise, a climate-driven forcing contributing to the formation of the RN transgressive dunefield cannot be ruled out.

5.1.3. From mid-Holocene to the present day

The end of the relative sea-level rise and coastline transgression in the mid-Holocene, and the onset of a drier climate at ~5 ka (Angulo et al., 2006 and Cruz et al., 2009, respectively) mark the reduction of the leading sources of sediment supply that promoted dune activity reaching the vicinity of Boqueirão Lake between ~11.5 ka and ~6.3 ka. This supply-dependent stabilization framework agrees with a study by Hugenholtz (2010) showing that parabolic dunes stabilize even under strong and steady winds, provided sediment supply diminish. After ~6 ka, relative sea-level variations in NE Brazil were negligible (Angulo et al., 2006) making coastal physiography and climate the essential forcings on dune formation in northeastern Brazil. SE trade winds in the mid-to late Holocene remained strong (Kim and Schneider, 2003; Kim et al., 2003), thus making precipitation the dominant factor controlling sediment availability from ~6 ka to the present day. However, the effect of changes in precipitation on sedimentation processes in the study area goes beyond the control of sand supply for dune activity. In an area also dominated by ephemeral rivers and lakes, it regulates fluvio-eolian interactions by controlling river flow competence affecting dune migration.

5.2. The Rio Grande do Norte coast under fluvio-eolian interplay

An understanding of the present-day geomorphic framework under the effects of fluvio-eolian interactions in the study area is discussed below. This discussion helps elucidate processes in the past that are explored in more detail using the Boqueirão Lake formation as a case study.

5.2.1. Modern deposits

Environmental forcings such as coastal orientation and physiography, wave and wind patterns, sediment availability, and accumulation space are essential controls on coastal eolian deposition (e.g., Lees, 2006; Giannini et al., 2007; Sawakuchi et al., 2008; Miot da Silva and Shulmeister, 2016). These factors are highly variable on the ~2900 km stretch of the NE coast of Brazil (Fig. 1 inset), thus explaining the irregular distribution of active and stabilized dunefields. Few or minor dunefields occur for approximately 1500 km on the eastern NE coast up to the Pernambuco State (Supplementary KMZ file). In turn, they become ubiquitous between the RN and the Maranhão States. The reasons for the concentration of dunefields in this northeastern coastal area can be varied and may involve a combination of the forcings mentioned above. However, we suggest two additional mechanisms that may also contribute to sand availability in the inner shelf that subsequently would be transported by wave action to the foreshore in the study area. The first is the decrease of the northbound longshore current from a maximum velocity of 105 cm s^{-1} to 25 cm s^{-1} (average speed of 6 cm s^{-1}) close to the Touros High (Fig. 1a; Hazin et al., 2008; Vital et al., 2010). The second involves the possible trapping of sediments by beach rock. Beach rock ridges may affect coastal dynamics by trapping sediments transported by the longshore drift and local circulation cells (Cooper, 1991). They are ubiquitous on the RN coast, which is considered one of the "hot spots" of beach rock in the world (Vousdoukas et al., 2007). In the RN state, beach rock formations are located parallel to the coast between the foreshore and 30 km offshore (Cabral Neto et al., 2010; Supplementary Fig. A.1). In the shoreline of the RN State, they can range in thickness and width from a few centimeters to almost 3 m, and from 2 to 50 m, respectively (Vieira et al., 2017). Conversely, beach rock ridges found offshore may reach up to 25 m in thickness, originating sub-aerial exposure in some locations (Cabral Neto et al., 2013). The contribution of the regional offshore beach rock ridges in confining sediments has not been regionally documented.

However, their effect on restricting fish dispersal suggests that sediment mobility may also be hindered by their walls, especially when the ridges are sub-aerially exposed or close to the water surface. In the RN State, fishermen go out to sea as far as 25-km distance from the coastline to catch seafood, confined by beach rock ridges, locally known as sand banks.

The source of sediments that accumulate in the inner shelf and ultimately feed the dunes can be related to at least two different processes. The first one is evidenced by the relatively unstable heavy minerals found only at the foreshore and active dunefield sands (Table 1b). These minerals most likely derived from southern coastal catchments such as the Potengi and Jundiaí rivers (Fig. 1a) that circumvent metamorphic and igneous rocks and were transported by the northward longshore drift. The second process involves recycling of sediments from the stabilized and active dunefields. During the wet season, sands eroded from stabilized or active deposits would be transported by the local rivers. Concurrently, active dune migration would be interrupted by flooding interdunes or by competent-flow drainages where saltating sands would fall into and then flushed to the Atlantic Ocean. Subsequently, sands brought to the foreshore would feed dune advancements that block or divert drainage pathways, thus promoting the formation of lakes, or shifts in the position of river mouths (Fig. 2b and a, respectively). These continuous fluvio-eolian cycles of sediment reworking highlight the link between climate and the geomorphic configuration in the study area.

5.2.2. Evidence of past fluvio-eolian interplay

In the study area, evidence of past fluvio-eolian interplay promoting geomorphic changes can be found in stabilized dunes and dammed lakes. They can be detected, for example, in marshes that are bounded by degraded parabolic ridges and depositional lobes (Fig. 2c), or in a paleochannel and a sandy layer detected in the dune-dammed Boqueirão Lake (Fig. 3b).

5.3. The Boqueirão Lake evolution

5.3.1. Fluvial deposition between ~11.2 ka and ~4.4 ka

The last recorded dune activity period in the vicinity of Boqueirão Lake was between 11.2 ± 0.9 ka and 6.3 ± 0.5 ka under the effect of the transgressive dunefield system. This interval is synchronous with the Holocene marine transgression and the regionally wetter climate period (Fig. 7a). Data from core BOQ/07/02 show that sand deposition became increasingly dominant over silt and clay between ~7.2 ka and ~4.4 ka (Fig. 7h). This suggests that an increase in sand content recorded in the core is related to a significant contribution of eolian processes before Boqueirão Lake was established. It is possible to establish a common eolian source of the dune succession profile sands with lake sediments during the ~7.2–4.4 ka period because the data show: (a) the same order of magnitude of the sand accumulation rate of 0.0515 cm yr^{-1} and 0.0426 cm yr^{-1}, respectively (Figs. 4g and 6b); and (b) similar grain size distribution (Fig. 5c). Also, it is unlikely that wind action distributed sand evenly in the 375 m-cross section of Boqueirão Lake (Fig. 3b) after the lake formation; the trapping effect of the lake waters would hinder the motion of eolian sands by creeping, saltation, or reptation. A study of eolian activity adjacent to Genggahai Lake in the Tibetan Plateau shows that eolian sands were transported and deposited into the lake for limited distances from the margins (Qiang et al., 2014). A numerical model of a saltating sand flow indicates that sand transport from dunes to lakes rarely exceeds 13 m farther than the lee of a dune, except for periods of high turbulence (Keen and Shane, 1990). Thus, during the wetter period, progressive dune weathering and erosion most likely left patches of relatively flat exposed sand terrain interspersed with

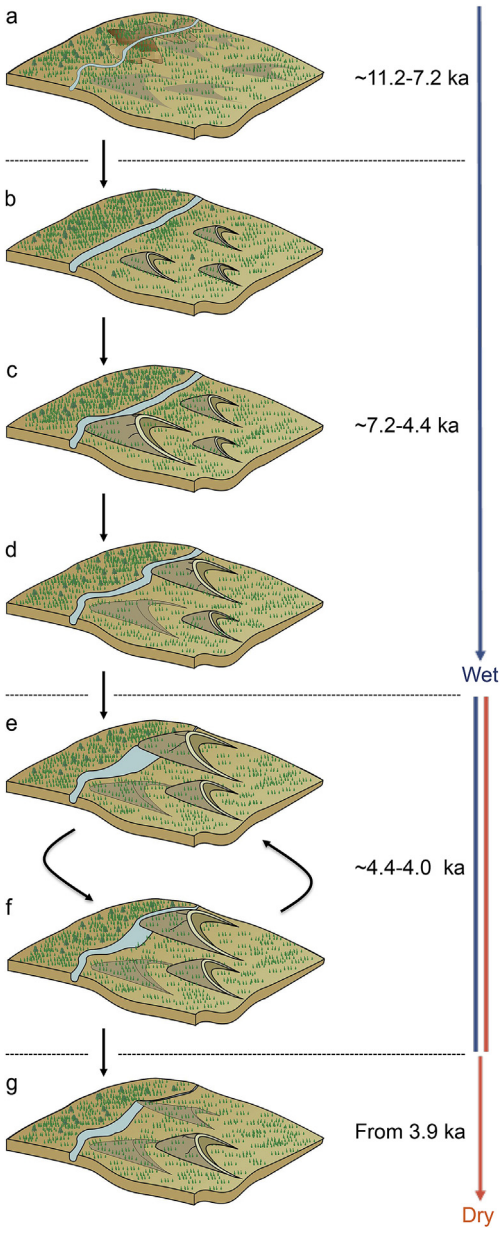

Fig. 8. Stages of the Boqueirão Lake landscape evolution revealed by fluvio-eolian interactions. (a) Increasingly wetter climate from ~11.2-7.2 ka benefits competent drainage flows and dune erosion. (b), (c), and (d) Peak of the wetter climate between ~7.2 ka and 4.4 ka promotes dune advancements and subsequent erosion. (e) and (f) Between ~4.4 ka and 4.0 k shifts from wetter to drier climate foster alternations between damming and dune-circumventing of Boqueirão River. (g) The increasingly drier climate conditions hinder dune advancements reaching Boqueirão Lake while decreasing the river competence flow to circumvent the existing dunes.

stabilized dunes (Fig. 8a and b), similar to what is currently observed NE of Boqueirão Lake (Fig. 2c). Under this framework, the competent-flow Boqueirão River would change pathway positions diverting from any advancing dunes until eolian sand transport diminished substantially at ~6.3 ka (Fig. 8 c and d).

However, the best evidence of past fluvial systems in the Boqueirão Lake area is revealed by sponge spicules of Class Demospongiae that appeared at ~7.2 ka peaking at ~4.4 ka (Fig. 7g). Class Demospongiae is associated with environments dominated by hard or sandy substrates that help its fixation (Frost, 2001; Frost et al., 2001). Also, these authors suggest that these sponges are

good indicators of well oxygenated riverine waters because this is a limiting factor for their survival. Our data show that the sandy deposition between ~7.2 ka and ~4.4 ka (Fig. 7h) is synchronous with low organic carbon content, and consequently, we could not analyze $\delta^{13}C$, $\delta^{15}N$, and C/N (Fig. 7c, d, and e, respectively) during this period. Hence, the fossil evidence confirms the prevalence of fluvial environments ~7.2–4.4 ka, consistent with the regional wetter climate.

5.3.2. Alternating fluvial and lacustrine deposition between ~4.4 and ~4.0 ka

Between ~4.4 ka and~ 4.0 ka shifts from fluvial to lacustrine environments were inferred from the interspersed peaks of sponge spicules and diatoms (Fig. 7g and f, respectively). This fluvial to lacustrine alternation is also consistent with the abrupt zig-zag fashion substitution of the sandy substrate to lake sediments, and with the geochemical data (Fig. 7h, c, d, and e). Additionally, this period is synchronous with changes from a wetter to a drier climate (Fig. 7a) and importantly, agrees with a transition from semi-humid to semi-arid forest biomes in NE Brazil because of declining moisture levels at ~4.2 ka (De Oliveira et al., 1999). These authors report a decrease in gallery forest taxa followed by an increase in caatinga and cerrado species in the Icatú River Valley.

We interpret this alternating fluvial and lacustrine deposition as a result of an oscillating Boqueirão River flow competence at times of limited dune activity. It seems likely that during the ~4.4–4.0 ka period Boqueirão River was still circumventing stabilized dunes, though episodic diminishing flow competence could benefit dune blockage by back-flooding the Boqueirão River valley (Fig. 8e). A subsequent wetter period could promote spillovers and river path diversion (Fig. 8f), reinstating a new cycle of competing fluvial and eolian processes. Damming would initially promote terrestrial organic matter accumulation derived from C4 vegetation from the lake margins as shown by $\delta^{13}C$ data (Fig. 7c). Subsequently, *Biomphalaria* sp. shells and possibly macrophytes would colonize the lake, enhancing the concentration of organic matter. An increasing C/N (Fig. 7e) and a lowering of $\delta^{13}C$ values attest to this premise. Also, the transition of depositional environments at ~4.4–4.0 ka shows increasing $\delta^{15}N$ values that are consistent with an increase in diatom abundance (Fig. 7d and f, respectively). Thus, our stable isotopes and geochemical data are consistent with the replacement of sponges by diatoms during the transition from fluvial to lacustrine systems. The interbedded layers of silt and sand (Fig. 6a and Supplementary Fig. A.3) corroborate this transition, suggesting events of higher and lower lake levels associated with alternating lacustrine and fluvial deposition.

5.3.3. Lacustrine deposition between ~3.9 ka and the present day

Starting at ~3.9 ka sponge spicules were substituted by lacustrine diatoms represented mainly by *M. smithii* var. *lacustris* and *Fragilaria* sp. These diatoms show contrasting habitats: periphytic, usually associated with macrophytes (Gaiser et al., 2010); and benthonic (Denys et al., 1991), respectively. Thus, the prevalence of one species over another in Boqueirão Lake indicates environmental conditions that influence physical limnological variables such as water flow, lake levels, or both. Also, from ~3.9 ka the fossil data are consistent with the geochemical record that show lower $\delta^{13}C$ and C/N values (Fig. 7c and e, respectively), indicating lotic water conditions caused by a predominance of algal organic matter associated with organic-rich sediments and low contribution of sand (Figs. 7h and 8g). Studies in paleolimnology have shown that these geochemical patterns are characteristic of lacustrine systems (Behling et al., 2001; Meyers, 2003). Subsequently, diatom density was drastically reduced after 3.1 ka and stabilized at 2.3 ka (Fig. 7f), when lake water presented more stable conditions of organic matter accumulation, as demonstrated by $\delta^{13}C$, $\delta^{15}N$, and C/N values (Fig. 7 c, d, and e, respectively). The absence of *Biomphalaria* sp. may suggest deeper waters in the area of the core sampling after 3.9 ka because this species thrives in shallow environments (Utzinger et al., 1997; Utzinger and Tanner, 2000). At ~2.3 ka, our data from organic additions coupled with low sand content (Fig. 7h) support the formation of an impervious Boqueirão Lake bottom that would hinder loss of volume to groundwater. In contrast, the unconsolidated and porous dune terrains of the eastern and northern shores present higher permeability and are thus prone to spillovers and water infiltration that affect lake water levels. In this respect, studies by Swinehart and Loope (1992) suggest that in lakes formed by dune blockage water levels remain stable because input usually equals output.

5.3.4. The Boqueirão Lake water level archive

This research complements previous studies using sediment cores from Boqueirão Lake correlating past lake levels with precipitation. Our analysis of a 2.85-m core enhances the study by Gomes et al. (2014) using diatom distribution from the upper 1.45-m depth core to assess lake levels, though there is a lack of chronological framework in their study. In turn, the lake level records of the last 3.0 ka and ~1.6 ka presented in Zocatelli et al. (2012) and Viana et al. (2014), respectively, are expanded to the early Holocene in our investigation. These authors used organic petrography and geochemistry, and grain size and diatom distribution, respectively, for their studies. Different from these previous contributions, our new study of the Boqueirão Lake evolution takes, for the first time, the changes in the eolian variable into consideration to assess paleoclimate and paleoenvironmental reconstructions. Also, in contrast with previous interpretations, our results indicate a rise in lake water levels concomitant with prevalent drier climate conditions. A corollary of these findings is that attempts to associate increasing lake water levels to periods of enhanced precipitation alone have to be considered with caution. The fluvio-eolian interplay mechanism presented in our study suggests a holistic perspective when investigating paleoenvironmental archives and geomorphic evolution rather than examining fluvial or eolian processes alone.

6. Conclusion

Our findings show that eolian dune development in the Rio Grande do Norte coast is associated with wetter, rather than the commonly associated drier periods for dune formation. Indeed, dune activity peaked between 11 ka and 6 ka with the formation of a transgressive dunefield under strong SE winds. During this period, a combination of a predominantly wetter climate and a rising relative sea level enhanced sediment availability. The interaction of advancing and stabilized dunes with the existing drainage depended on the intensity of dune activity and riverine flow competence, thus promoting river-dammed lakes or diversion of river pathways. This fluvio-eolian interplay is illustrated by the Boqueirão Lake evolution using sedimentological, geochemical and microfossil data. Our study reveals that the correlation of lake levels of Boqueirão Lake with a wetter climate is not straightforward. Contrary to previously reported findings, this new study evidences that the formation of this lake is a result of the Boqueirão River damming by dunes at times of diminishing rains in the mid-Holocene. Additionally, the high abundance of lake-diatoms in Boqueirão Lake is consistent with a predominantly drier period from 4 ka to 1 ka. The interaction of fluvial and eolian systems responsible for the formation of this lake continued in the late Holocene shaping the regional landscape, under the sediment supply forcing constrained by climate and coastal physiography.

Paleoclimate studies based on lake water levels in this region can only be understood in light of continual interplay of fluvial, eolian, and lacustrine processes. The findings in this paper may guide future research in the area to shed light on sedimentary processes during the Holocene. New studies may include, for example, the dating of the offshore beach rock to determine the paleo-coastline chronology that could help elucidate the reasons for the onset of the predominantly eolian deposition after the LGM.

Acknowledgments

We thank Elaine Sinfronio, Jordana Zampelli, and Marco Antônio Netto Chamadoira for helping with sedimentological analysis and with the final regional map. We show appreciation for Paulo Eduardo de Oliveira, Paula Garcia Carvalho do Amaral and technicians from the Geoscience Laboratory at the University of Guarulhos for helping with micropaleontological analysis. We acknowledge the Geochemistry and Geotectonics department from the Institute of Geosciences at the University of São Paulo for providing funds under the CAPES-PROEX program. We also thank Fundação de Amparo à Pesquisa do Estado de São Paulo (FAPESP) for funding this research under projects FAPESP 2009/54232-4 and EMU 09/53988-8. This study was undertaken as part of the Laboratório Misto Internacional "Paleoclimatologia TropicaL, Traçadores e Variabilidade" – PALEOTRACES" (IRD-UFF-USP) and the Dimensions US-BIOTA-São Paulo program grant 2013/50260: A multidisciplinary framework for biodiversity prediction in the Brazilian Atlantic forest hotspot. We are grateful to Charles Levesque for providing language help. Finally, we would like to thank the editor, Prof. Xiaoping Yang, and the two anonymous reviewers for their helpful comments and suggestions that contributed to improving this manuscript.

Appendix A. Supplementary data

Supplementary data related to this article can be found at https://doi.org/10.1016/j.quascirev.2018.07.022.

References

Aitken, M.J., 1998. An Introduction to Optical Dating. Oxford University Press, New York.
Al-Masrahy, M.A., Mountney, N.P., 2015. A classification scheme for fluvial–aeolian system interaction in desert-margin settings. Aeolian Res. 17, 67–88.
Amarante, O.A.C., Silva, F.J.L., Rios Filho, L.G., 2003. Potencial Eólico do Estado do Rio Grande do Norte, Projeto de Pesquisa e Desenvolvimento COSERN/ANEL. http://www.cresesb.cepel.br/index.php?section=publicacoes&task=livro&cid=1. (Accessed 10 November 2016).
Angelim, L.A.A., Medeiros, V.C., Nesi, J.R., 2006. Mapa Geológico Do Estado Do Rio Grande Do Norte, Escala 1:500.000, Recife,CPRM/FAPERN. http://geosgb.cprm.gov.br/. (Accessed 25 October 2016).
Angnuureng, D.B., Almar, R., Senechal, N., Castelle, B., Addo, K.A., Marieu, V., Ranasinghe, R., 2017. Shoreline resilience to individual storms and storm clusters on a meso-macrotidal barred beach. Geomorphology 290, 265–276.
Angulo, R.J., Lessa, G.C., de Souza, M.C., 2006. A critical review of mid-to late-Holocene sea-level fluctuations on the eastern Brazilian coastline. Quat. Sci. Rev. 25, 486–506.
Arnold, L.J., Roberts, R.G., 2009. Stochastic modeling of multi-grain equivalent dose (De) distributions: implications for OSL dating of sediment mixtures. Quat. Geochronol. 4, 204–230.
Arthington, A.H., Burton, H.B., Williams, R.W., Outridge, P.M., 1986. Ecology of humic and non-humic dune lakes, Fraser Island, with emphasis on the effects of sand infilling in Lake Wabby. Mar. Freshw. Res. 37, 743–764.
Bateman, M.D., Boulter, C.H., Carr, A.S., Frederick, C.D., Peter, D., Wilder, M., 2007. Preserving the palaeoenvironmental record in drylands: bioturbation and its significance for luminescence-derived chronologies. Sediment. Geol. 195, 5–19.
Battarbee, R.W., 1986. Diatoms analysis. In: Berglund, B.E. (Ed.), Handbook of Holocene Palaeoecology and Palaeohydrology. John Wiley & Sons, New York, pp. 527–570.
Behling, H., Keim, G., Irion, G., Junk, W., Mello, J.N., 2001. Holocene environmental changes in the central amazon basin inferred from lago Calado (Brazil). Palaeogeogr. Palaeoclimatol. Palaeoecol. 173, 87–101.
Bertrand, G., Hirata, R., Auler, A., Cruz, F., Cary, L., et al., 2017. Groundwater isotopic data as potential proxy for Holocene paleohydroclimatic and paleoecological models in NE Brazil. Palaeogeogr. Palaeoclimatol. Palaeoecol. 469, 92–103.
Bittencourt, A.C.D.S.P., Dominguez, J.M.L., Martin, L., Silva, I.R., 2005. Longshore transport on the northeastern Brazilian coast and implications to the location of large scale accumulative and erosive zones: an overview. Mar. Geol. 219, 219–234.
Boski, T., Bezerra, F.H., de Fátima Pereira, L., Souza, A.M., Maia, R.P., Lima-Filho, F.P., 2015. Sea-level rise since 8.2 ka recorded in the sediments of the potengi–Jundiai Estuary, NE Brasil. Mar. Geol. 365, 1–13.
Bullard, J.E., Livingstone, I., 2002. Interactions between aeolian and fluvial systems in dryland environments. Area 34, 8–16.
Bullard, J.E., McTainsh, G.H., 2003. Aeolian-fluvial interactions in dryland environments: examples, concepts and Australia case study. Prog. Phys. Geogr. 27, 471–501.
Buynevich, I.V., Souza Filho, P.W.M., Asp, N.E., 2010. Dune advance into a coastal forest, equatorial Brazil: a subsurface perspective. Aeolian Res. 2, 27–32.
Cabral Neto, I., Córdoba, V.C., Vital, H., 2010. Petrografia de beachrock em zona costa afora adjacente ao litoral norte do Rio Grande do Norte, Brasil. Quat. Environ. Geosci. 2, 12–18.
Cabral Neto, I., Córdoba, V.C., Vital, H., 2013. Morfologia, Microfaciologia e Diagênese de Beachrocks Costa-Afora Adjacentes à Costa Norte do Rio Grande do Norte, Brasil. Geociencias 32, 471–490.
Caldas, L.H.O., Stattegger, K., Vital, H., 2006. Holocene sea-level history: evidence from coastal sediments of the northern Rio Grande do Norte coast, NE Brazil. Mar. Geol. 228, 39–53.
Carter, R.W.G., 1990. The geomorphology of coastal dunes in Ireland. Catena Suppl. 18, 31–40.
Christiansen, C., Dalsgaard, K., Moller, J.T., Bowman, D., 1990. Coastal dunes in Denmark. Chronology in relation to sea-level. Catena Suppl. 18, 61–70.
Cooper, W.S., 1958. Coastal Sand Dunes of Oregon and Washington, Geological Society of America Memoirs 72. Waverly Press Inc., Baltimore.
Cooper, J.A.G., 1991. Beachrock formation in low latitudes: implications for coastal evolutionary models. Mar. Geol. 98, 145–154.
Cruz, F.W., Vuille, M., Burns, S.J., Wang, X., Cheng, H., Werner, M., Nguyen, H., 2009. Orbitally driven east–west antiphasing of South American precipitation. Nat. Geosci. 2, 210–214.
Cunningham, A.C., Wallinga, J., Minderhoud, P.S., 2011. Expectations of scatter in equivalent-dose distributions when using multi-grain aliquots for OSL dating. Geochronometria 38, 424–431.
De Miranda, L.B., Bergamo, A.L., De Castro, B.M., 2005. Interactions of river discharge and tidal modulation in a tropical estuary, NE Brazil. Ocean Dynam. 55, 430–440.
De Oliveira, P.E., Barreto, A.M.F., Suguio, K., 1999. Late Pleistocene/Holocene climatic and vegetational history of the Brazilian caatinga: the fossil dunes of the middle Sao Francisco River. Palaeogeogr. Palaeoclimatol. Palaeoecol. 152, 319–337.
Denys, L., Verbruggen, C., Kiden, P., 1991. Palaeolimnological aspects of a late-glacial shallow lake in sandy flanders. Belgium. Hydrobiol. 214, 273–278.
Dietze, M., Kreutzer, S., Burow, C., Fuchs, M.C., Fischer, M., Schmidt, C., 2016. The abanico plot: visualising chronometric data with individual standard errors. Quat. Geochronol. 31, 12–18.
Diniz Filho, J.B., De Queiroz, M.A., Do Nascimento, J.M.S., De Melo, F.T.L., 2005. Estudo do Aquífero Freático da Região da Laguna de Guaraíra-Tibau do Sul/RN. Estud. Geol. 15, 68.
Friedman, G.M., Sanders, J.E., Kopaska-Merkel, D.C., 1992. Principles of Sedimentary Deposits. Macmillan Publishing Company, New York.
Frost, T.M., 2001. Freshwater sponges. In: Smol, J.P., Birks, H.J.B., Last, W.M. (Eds.), Tracking Environmental Change Using Lakes Sediments 3. Kluwer Academic Publishers, London, pp. 253–263.
Frost, T.M., Reiswig, H.M., Ricciardi, A., 2001. Porifera. In: Thorp, J.P., Covich, A.P. (Eds.), Ecology and Classification of North American Freshwater Invertebrates, 2º Ed. Academic Press, New York, pp. 97–133.
Gaiser, E., La Hée, J.M., Tobias, F.A., Wachnicka, A.H., 2010. *Mastogloia smithii* var. *lacustris* Grun.: a structural engineer of calcareous mats in karstic subtropical wetlands. Proc. Acad. Nat. Sci. Phila. 160, 99–112.
Galbraith, R.F., Roberts, R.G., Laslett, G.M., Yoshida, H., Olley, J.M., 1999. Optical dating of single and multiple grains of quartz from jinmium rock shelter, northern Australia, part 1, experimental design and statistical models. Archaeometry 41, 339–364.
Galehouse, J.S., 1971. Point counting. In: Carver, R.E. (Ed.), Procedures in Sedimentary Petrology. Wiley, New York, pp. 385–407.
Garzanti, E., Vermeesch, P., Andò, S., Lustrino, M., Padoan, M., Vezzoli, G., 2014. Ultra-long distance littoral transport of orange sand and provenance of the Skeleton Coast Erg (Namibia). Mar. Geol. 357, 25–36.
GEBCO, 2003. General Bathymetric Chart of the Oceans Digital Atlas. IOC, IHO and BODC. "Centenary Edition of the GEBCO Digital Atlas", Published on CD-rom on Behalf of the Intergovernmental Oceanographic Commission and the International Hydrographic Organization as Part of the General Bathymetric Chart of the Oceans. British Oceanographic Data Centre, Liverpool.
Guedes, C.C.F., Giannini, P.C.F., Sawakuchi, A.O., DeWitt, R., de Aguiar Â.P, V., 2017. Weakening of northeast trade winds during the Heinrich stadial 1 event recorded by dune field stabilization in tropical Brazil. Quat. Res. 88, 369–381.
Giannini, P.C., Sawakuchi, A.O., Martinho, C.T., Tatumi, S.H., 2007. Eolian depositional episodes controlled by Late Quaternary relative sea level changes on the Imbituba–Laguna coast (southern Brazil). Mar. Geol. 237, 143–168.

Guérin, G., Mercier, N., Adamiec, G., 2011. Dose-rate conversion factors: update. Anc. TL 29, 5–8.
Gomes, D.F., Albuquerque, A.L.S., Torgan, L.C., Turcq, B., Sifeddine, A., 2014. Assessment of a diatom-based transfer function for the reconstruction of lake-level changes in Boqueirão Lake, Brazilian Nordeste. Palaeogeogr. Palaeoclimatol. Palaeoecol. 415, 105–116.
Harley, M.D., Turner, I.L., Kinsela, M.A., Middleton, J.H., Mumford, P.J., et al., 2017. Extreme coastal erosion enhanced by anomalous extratropical storm wave direction. Sci. Rep. 7, 6033.
Hazin, F.H.V., Wor, C., Oliveira, J.E.L., Hamilton, S., Travassos, P., Geber, F., 2008. Resultados obtidos por meio do fundeio de um correntógrafo na plataforma continental do Estado do Rio Grande do Norte, Brasil. Arq. Cienc. Mar 41, 30–35.
Hesp, P.A., 2013. Conceptual models of the evolution of transgressive dune field systems. Geomorphology 199, 138–149.
Hesp, P.A., Martinez, M., da Silva, G.M., Rodríguez-Revelo, N., Gutierrez, et al., 2011. Transgressive dunefield landforms and vegetation associations, Doña Juana, Veracruz, Mexico. Earth Surf. Process. Landforms 36, 285–295.
Hogg, A.G., Hua, Q., Blackwell, P.G., Niu, M., Buck, C.E., et al., 2013. SHCal13 southern Hemisphere calibration, 0–50,000 Years cal BP. Radiocarbon 55, 1889–1903.
Holland, H.D., Gottfried, D., 1955. The effect of nuclear radiation on the structure of zircon. Acta Crystallogr. 8, 291–300.
Hollands, C.B., Nanson, G.C., Jones, B.G., Bristow, C.S., Price, D.M., Pietsch, T.J., 2006. Aeolian–fluvial interaction: evidence for Late Quaternary channel change and wind-rift linear dune formation in the northwestern Simpson Desert, Australia. Quat. Sci. Rev. 25, 142–162.
Hugenholtz, C.H., 2010. Topographic changes of a supply-limited inland parabolic sand dune during the incipient phase of stabilization. Earth Surf. Process. Landforms 35, 1674–1681.
Hugenholtz, C.H., Wolfe, S.A., 2005. Biogeomorphic model of dunefield activation and stabilization on the northern Great Plains. Geomorphology 70, 53–70.
Illenberger, W.K., 1996. The geomorphologic evolution of the Wilderness dune cordons, South Africa. Quat. Int. 33, 11–20.
Kadlec, J., Kocurek, G., Mohrig, D., Shinde, D.P., Murari, M.K., Varma, V., Stehlík, F., Benes, V., Singhvi, A.K., 2015. Response of fluvial, aeolian, and lacustrine systems to late Pleistocene to Holocene climate change, Lower Moravian Basin, Czech Republic. Geomorphology 232, 193–208.
Keen, K.L., Shane, L.C.K., 1990. A continuous record of Holocene eolian activity and vegetation change at Lake Ann, east-central Minnesota. Geol. Soc. Am. Bull. 102, 1646–1657.
Kim, J.H., Schneider, R.R., 2003. Low-latitude control of interhemispheric sea-surface temperature contrast in the tropical Atlantic over the past 21 kyears: the possible role of SE trade winds. Clim. Dynam. 21, 337–347.
Kim, J.H., Schneider, R.R., Mulitza, S., Müller, P.J., 2003. Reconstruction of SE trade-wind intensity based on seasurface temperature gradients in the Southeast Atlantic over the last 25 kyr. Geophys. Res. Lett. 30 (22).
Kocurek, G., 1999. The aeolian rock record. In: Goudie, A.S., Livingstone, I., Stokes, S. (Eds.), Aeolian Environments, Sediments and Landforms. Wiley, New York, pp. 239–259.
Kousky, V.E., 1979. Frontal influences on northeast Brazil. Mon. Weather Rev. 107, 1140–1153.
Krapf, C.B.E., 2018. Distribution of transported regolith along the Skeleton Coast Erg of Namibia: a complex story of fluvio-aeolian interaction. In: Krapf, C.B.E., Keeling, J., Petts, A. (Eds.), Proceedings for the 5th Australian Regolith Geoscientists Association Conference. South Australia, Adelaide, pp. 39–40.
Krapf, C.B.E., Stollhofen, H., Stanistreet, I.G., 2003. Contrasting styles of ephemeral river systems and their interaction with dunes of the Skeleton Coast erg (Namibia). Quat. Int. 104, 41–52.
Langford, R.P., 1989. Fluvial-aeolian interactions: Part I, modern systems. Sedimentology 36, 1023–1035.
Langford, R.P., Chan, M.A., 1989. Fluvial-aeolian interactions: Part II, ancient systems. Sedimentology 36, 1037–1051.
Lees, B., 2006. Timing and formation of coastal dunes in northern and eastern Australia. J. Coast Res. 22, 78–89.
Lees, B.G., Hayne, M., Price, D., 1993. Marine transgression and dune initiation on western Cape York, northern Australia. Mar. Geol. 114, 81–89.
Liu, B., Coulthard, T.J., 2015. Mapping the interactions between rivers and sand dunes: implications for fluvial and aeolian geomorphology. Geomorphology 231, 246–257.
Liu, B., Coulthard, T.J., 2017. Modelling the interaction of aeolian and fluvial processes with a combined cellular model of sand dunes and river systems. Comput. Geosci. 106, 1–9.
Lomax, J., Hilgers, A., Twidale, C.R., Bourne, J.A., Radtke, U., 2007. Treatment of broad palaeodose distributions in OSL dating of dune sands from the western Murray Basin, South Australia. Quat. Geochronol. 2, 51–56.
Loope, D.B., Swinehart, J.B., Mason, J.P., 1995. Dune-dammed paleovalleys of the Nebraska Sand Hills: intrinsic versus climatic controls on the accumulation of lake and marsh sediments. Geol. Soc. Am. Bull. 104, 396–406.
Loope, D.B., Swinehart, J.B., 2000. Thinking like a dune field: geologic history in the Nebraska sand Hills. Gt. Plains Res. 486, 5–35.
Loope, W.L., Fisher, T.G., Jol, H.M., Goble, R.J., Anderton, J.B., Blewett, W.L., 2004. A Holocene history of dune-mediated landscape change along the southeastern shore of Lake Superior. Geomorphology 61, 303–322.
Macdonald, W.G., Rozendaal, A., de Meijer, R.J., 1997. Radiometric characteristics of heavy mineral deposits along the west coast of South Africa. Miner. Deposita 32, 371–381.
Mason, J.P., Swinehart, J.B., Loope, D.B., 1997. Holocene history of lacustrine and marsh sediments in a dune-blocked drainage, southwestern Nebraska Sand Hills, USA. J. Paleolimnol. 17, 67–83.
Mason, J.A., Swinehart, J.B., Hanson, P.R., Loope, D.B., Goble, R.J., Miao, X., Schmeisser, R.L., 2011. Late pleistocene dune activity in the central great plains, USA. Quat. Sci. Rev. 30, 3858–3870.
Meyers, P.A., 2003. Applications of organic geochemistry to paleolimnological reconstructions: a summary of examples from the Laurentian Great Lakes. Org. Geochem. 34, 261–289.
Milne, G.A., Long, A.J., Bassett, S.E., 2005. Modelling holocene relative sea-level observations from the Caribbean and south America. Quat. Sci. Rev. 24, 1183–1202.
Miot da Silva, G., Shulmeister, J., 2016. A review of coastal dunefield evolution in southeastern queensland. J. Coast Res. 75, 308–312.
Mohanty, A.K., Sengupta, D., Das, S.K., Vijayan, V., Saha, S.K., 2004. Natural radioactivity in the newly discovered high background radiation area on the eastern coast of Orissa, India. Radiat. Meas. 38, 153–165.
Montade, V., Ledru, M.P., Burte, J., Martins, E.S.P.R., Verola, C.F., et al., 2014. Stability of a Neotropical microrefugium during climatic instability. J. Biogeogr. 41, 1215–1226.
Mulitza, S., Chiessi, C.M., Schefuß, E., Lippold, J., Wichmann, D., et al., 2017. Synchronous and proportional deglacial changes in Atlantic Meridional Overturning and northeast Brazilian precipitation. Paleoceanography 32. PA003084.
Munsell Soil Color Charts, 1992. Munsell Color, Newburgh.
Murray, A.S., Wintle, A.G., 2003. The single aliquot regenerative dose protocol: potential for improvements in reliability. Radiat. Meas. 37, 377–381.
Murray-Wallace, C.V., Woodroffe, C.D., 2014. Quaternary Sea-level Changes: a Global Perspective. Cambridge University Press, New York.
Nathan, R.P., Mauz, B., 2008. On the dose-rate estimate of carbonate-rich sediments for trapped charge dating. Radiat. Meas. 43, 14–25.
Novello, V.F., Cruz, F.W., Karmann, I., Burns, S.J., Stríkis, N.M., et al., 2012. Multidecadal climate variability in Brazil's Nordeste during the last 3000 years based on speleothem isotope records. Geophys. Res. Lett. 39, 23.
Padilla, E.M., Alsina, J.M., 2017. Transfer and dissipation of energy during wave group propagation on a gentle beach slope. J. Geophys. Res.: Oceans 122, 6773–6794.
Prescott, J.R., Stephan, L.G., 1982. The contribution of cosmic radiation to the environmental dose for thermoluminescence dating. In: Proceedings of the Second Specialist Seminar on Thermoluminescence Dating, 6. Council of Europe, Strasbourg, pp. 17–25.
Pye, K., Bowman, G.M., 1984. The Holocene marine transgression as a forcing function in episodic dune activity on the eastern Australian coast. In: Thom, B.G. (Ed.), Coastal Geomorphology in Australia. Academic Press, Sydney, pp. 179–196.
Qiang, M., Liu, Y., Jin, Y., Song, L., Huang, X., Chen, F., 2014. Holocene record of eolian activity from Genggahai Lake, northeastern Qinghai-Tibetan plateau, China. Geophys. Res. Lett. 41, 589–595.
Rawling, J.E., Hanson, P.R., Young, A.R., Attig, J.W., 2008. Late Pleistocene dune construction in the central sand plain of Wisconsin, USA. Geomorphology 100, 494–505.
Roskin, J., Bookman, R., Friesem, D.E., Vardi, J., 2017. A late Pleistocene linear dune dam record of aeolian-fluvial dynamics at the fringes of the northwestern Negev dunefield. Sediment. Geol. 353, 76–95.
Roy, P.S., Thom, B.G., 1981. Late quaternary marine deposition in new south wales and southern queensland – an evolutionary model. J. Geol. Soc. Aust. 28, 471–490.
Sawakuchi, A.O., Kalchgruber, R., Giannini, P.C.F., Nascimento, D.R., Guedes, C.C.F., Umisedo, N.K., 2008. The development of blowouts and foredunes in the Ilha Comprida barrier (Southeastern Brazil): the influence of Late Holocene climate changes on coastal sedimentation. Quat. Sci. Rev. 27, 2076–2090.
Schettini, C.A.F., Toldo Jr., E.E., 2004. Fine sediment transport modes in the Itajaí-Açu estuary, Southern Brazil. J. Coast. Res. SI 39, 515–519.
Schmieder, J., Fritz, S.C., Grimm, E.C., Jacobs, K.C., Brown, K.J., Swinehart, J.B., Porter, S.C., 2013. Holocene variability in hydrology, vegetation, fire, and eolian activity in the Nebraska Sand Hills, USA. Holocene 23, 515–527.
Sifeddine, A., Albuquerque, A.L.S., Ledru, M.P., Turcq, B., Knoppers, B., et al., 2003. A 21 000 cal years paleoclimatic record from Caçó Lake, northern Brazil: evidence from sedimentary and pollen analyses. Palaeogeogr. Palaeoclimatol. Palaeoecol. 189, 25–34.
Singhvi, A.K., Porat, N., 2008. Impact of luminescence dating on geomorphological and palaeoclimate research in drylands. Boreas 37, 536–558.
Sloss, C.R., Murray-Wallace, C.V., Jones, B.G., 2007. Holocene sea-level change on the southeast coast of Australia: a review. Holocene 17, 999–1014.
Stevenson, R.J., Rollins, S.L., 2006. Ecological Assessments with Benthic Algae. In: Hauer, F.R., Lamberti, G.A. (Eds.), Methods in Stream Ecology, second ed. Elsevier, London, pp. 785–804.
Suanez, S., Cariolet, J.M., Cancouët, R., Ardhuin, F., Delacourt, C., 2012. Dune recovery after storm erosion on a high-energy beach: vougot Beach, Brittany (France). Geomorphology 139, 16–33.
Svendsen, J., Stollhofen, H., Krapf, C.B., Stanistreet, I.G., 2003. Mass and hyperconcentrated flow deposits record dune damming and catastrophic breakthrough of ephemeral rivers, Skeleton Coast Erg, Namibia. Sediment. Geol. 160, 7–31.
Swinehart, J.B., Loope, D.B., 1992. A giant Dune-dammed lake on the north platte river, Nebraska. Geol. Soc. Am., Abstr. Progr. 24, 7.

Teller, J.T., Lancaster, N., 1986. Lacustrine sediments at narabeb in the central namib desert, Namibia. Palaeogeogr. Palaeoclimatol. Palaeoecol. 56, 177–195.
Tsoar, H., Levin, N., Porat, N., Maia, L., Herrmann, H., Tatumi, S.H., Sales, V.C., 2009. The effect of climate change on the mobility and stability of coastal sand dunes in Ceará State (NE Brazil). Quat. Res. 71, 217–226.
Utzinger, J., Mayobana, C., Smith, T., Tanner, M., 1997. Spatial microhabitat selection by *Biomphalaria pfeifferi* in a small perennial river in Tanzania. Hydrobiol. (Sofia) 356, 53–60.
Utzinger, J., Tanner, M., 2000. Microhabitat preferences of *Biomphalaria pfeifferi* and *Lymnaea natalensis* in a natural and a man-made habitat in southeastern Tanzania. Meml. Inst. Oswaldo Cruz Rio J 95, 287–294.
Viana, J.C.C., Sifeddine, A., Turcq, B., Albuquerque, A.L.S., Moreira, L.S., Gomes, D.F., Cordeiro, R.C., 2014. A late Holocene paleoclimate reconstruction from Boqueirão Lake sediments, northeastern Brazil. Palaeogeogr. Palaeoclimatol. Palaeoecol. 415, 117–126.
Vieira, M.M., Sial, A.N., De Ros, L.F., Morad, S., 2017. Origin of holocene beachrock cements in northeastern Brazil: evidence from carbon and oxygen isotopes. J. S. Am. Earth Sci. 79, 401–408.
Vital, H., Amaro, V.E., Silveira, I.D., 2004. Coastal erosion on the Rio Grande do norte state (northeastern Brazil): causes and factors versus effects and associated processes. J. Coast Res. 1306–1309.
Vital, H., Gomes, M.P., Tabosa, W.F., Frazão, E.P., Santos, C.L.A., Júnior, P., Saraiva, J., 2010. Characterization of the Brazilian continental shelf adjacent to Rio Grande do Norte state, NE Brazil. Braz. J. Oceanogr. 58, 43–54.
Vital, H., da Silveira, I.M., Tabosa, W.F., Lima, Z.M.C., Lima-Filho, F.P., de Souza, F.E.S., Chaves, M.S., Pimenta, F.M., Gomes, M.P., 2016. Beaches of Rio Grande do norte. In: Short, A.D., Klein, A.H.F. (Eds.), Brazilian Beach Systems. Springer International Publishing, pp. 201–230.
Vousdoukas, M.I., Velegrakis, A.F., Plomaritis, T.A., 2007. Beachrock occurrence, characteristics, formation mechanisms and impacts. Earth Sci. Rev. 85, 23–46.
Wentworth, C.K., 1922. A scale of grade and class terms for clastic sediments. J. Geol. 30, 377–392.
Zocatelli, R., Turcq, B., Boussafir, M., Cordeiro, R.C., Disnar, J.R., Costa, R.L., Sifeddine, A., Albuquerque, A.L.S., Bernardes, M.C., Jacob, J., 2012. Late Holocene paleoenvironmental changes in Northeast Brazil recorded by organic matter in lacustrine sediments of Lake Boqueirão. Palaeogeogr. Palaeoclimatol. Palaeoecol. 363, 127–1.